Drug-mediated metabolic tipping: antimicrobial resistance shifts in a mixed-species community

Robert E. Beardmore[1+*], Emily Cook[1+], Susanna Nilsson[1],
Adam R. Smith[3], Anna Tillmann[4], Brooke D. Esquivel[3]
Ken Haynes[1†], Neil A. R. Gow[4], Alistair J. P. Brown[4],
Theodore C. White[3] and Ivana Gudelj[1*]

[1]Biosciences, University of Exeter, Exeter, UK,
[3]School of Biological Sciences, University of Missouri at Kansas City, Kansas City, MO, USA
[4]Institute of Medical Sciences, Foresterhill, University of Aberdeen, Aberdeen, UK

[+]Authors contributed equally;
[*]To whom correspondence should be addressed;
E-mails: r.e.beardmore@exeter.ac.uk; i.gudelj@exeter.ac.uk
[†] Passed away 19th March 2018

Microbes rarely exist in isolation, rather, they form intricate multi-species communities that colonise our bodies and inserted medical devices. However, the efficacy of antimicrobials is measured in clinical laboratories exclusively using microbial monocultures. Here, to determine how multi-species interactions mediate selection for resistance during antibiotic treatment, particularly following drug withdrawal, we study a laboratory community consisting of two microbial pathogens. Single-species dose responses are a poor predictor of community dynamics during treatment so, to better understand those dynamics, we introduce the concept of a dose-response mosaic, a multi-dimensional map that indicates how species' abundance is affected by changes in abiotic conditions. We study the dose response mosaic of a two-species community possessing a 'Gene×Gene×Environment×Environment' ecological interaction whereby *Candida glabrata*, which is resistant to the antifungal drug fluconazole, competes for survival with *Candida albicans*, which is susceptible to fluconazole. The mosaic comprises several zones that delineate abiotic conditions where each species dom-

inates. Zones are separated by loci of bifurcations and tipping points that identify what environmental changes can trigger the loss of either species. Observations of the laboratory communities corroborated theory, showing that changes in both antibiotic concentration and nutrient availability can push populations beyond tipping points, thus creating irreversible shifts in community composition from drug sensitive to drug resistant species. This has an important consequence: resistant species can increase in frequency even if an antibiotic is withdrawn because, unwittingly, a tipping point was passed during treatment.

Antimicrobial resistance poses a formidable challenge for medicine with resistance to all but the most recently discovered antibiotics encountered in clinical and agricultural practice (*1*). Seeking behavioural changes in antibiotic prescription to control resistance is a field of active theoretical, laboratory and clinical research. Importantly, it has been mooted that resistance could be eliminated using evolution-aware strategies that reverse the arrow of time (*2*). But is drug resistance reversible? And if not, why not?

Antibiotic cycling, whereby different antibiotics are prioritised and restricted through time, can lead to the reversal of resistance if resistant microbes pay the price for their abilities to resist by having reduced fitness when drugs are not around (*3, 4*). This idea has been tested clinically, with mixed outcomes. Restricting use can reduce resistance (*5,6*) though not always (*7*) and, perversely, increases in resistance have been observed following drug restrictions (*6, 8*). Thus clinical strategies that cycle antibiotics have unpredictable effects: they can work (*9–13*) but sometimes they fail (*14, 15*). It is unclear why a self-evidently worthwhile strategy of antibiotic withdrawal would not reduce resistance. An absence of fitness costs of resistance (*16*) is one potential explanation but, in microbial communities, as we now explain, there is another.

Our explanation is this. For simplicity, imagine a microbial community dominated by two species, S and R. Assume the former is sensitive to an antimicrobial and the latter is resistant. Suppose S can invade, and displace, R in the absence of drug and R can invade and displace S in the presence of drug; in this case the drug resistance phenotype of the community is reversible. However, if, now in a different community, R invades and displaces S in the presence of drug but, in the drug's absence, the community exhibits a frequency dependent bistability (*17*) whereby either R *or* S can

dominate, then this community need not have reversible resistance. Here, application of drug forces R to become dominant and the inability of S to always re-invade following withdrawal could cause resistance not to reverse. Now a tipping point is said to occur when S can no longer invade and we provide theoretical mechanisms and microbial data demonstrating how the irreversibility of resistance can arise through tipping.

Metagenomic analyses are rapidly improving our understanding of microbial communities. We now know that antibiotics affect communities in load (*18*) and in diversity (*19*) and, intriguingly, the removal of antibiotic sometimes (*20, 21*) but not always (*22, 23*) restores the community to its original, pre-treated composition. However, selection for resistance within communities is poorly understood because key pharmacological indicators, like the minimal inhibitory concentration (MIC), dose-responses, between-antibiotic drug interactions and costs of resistance are measured in single-species assays. These assays ignore the antibiotic's true context: while microbes can exist as single-species populations, in bloodstream infections, say, most real-world microbes thrive in communities. Why, therefore, should a single-species understanding of microbial responses to antibiotics completely explain resistance progression on the skin, in the gut or a hospital ward?

To support this view, here we show that single-species resistance measures can be poor predictors of resistance in a synthetic microbial community both during treatment, and after antibiotic withdrawal, because of a hitherto unobserved phenomenon: communities can have tipping points when abiotic parameters like treatment duration, antibiotic dose and nutrient availability vary. For example, clinicians vary dosing regimens (*24–26*) and treatment duration (*27*) of critically ill patients while nutrient availability, in the form of glucose concentration, can vary from $0.01 - 0.28\%$ in urine (*28*) to $0.1 - 2.7\%$ in blood with substantial daily variation (*29, 30*). The impact of this on drug resistance is unknown.

We explore resistance and abiotic variation in the simplest possible community of two species, *Candida albicans* and *Candida glabrata*. Both are commensal microbes found together in the microbiota of healthy individuals but they are also opportunistic pathogens causing mucosal infections (*31*) and life-threatening disseminated infections among immunocompromised patients (*32*). Difficult to diagnose, *Candida* infections are associated with high mortality rates, ranging from 46-75% for *Candidiasis* in the bloodstream (*33–35*). Strikingly, as many people die each year from the top ten invasive fungal diseases, including candidiasis, as do from tuberculosis or malaria (*33*). Apart from

its substantial impact on human health, our community treatment model is suited to studying drug withdrawal dynamics because *C. glabrata* infections are relatively unresponsive to the most frequently used antifungal drug fluconazole, while *C. albicans* is sensitive to fluconazole (*36*). Monoculture dose response assays demonstrate this for our study strains at clinical doses (Supporting Fig. S2).

We determined temporal dynamics of the *Candida* species empirically by monitoring their relative frequencies. For this we co-cultured both in shaken, 96-well plates containing liquid growth media supplemented with glucose and fluconazole. The plates were inoculated with a mixture of fluorescently labelled *C. albicans*, at proportion f, and *C. glabrata*, at proportion $1-f$. After 24h of growth (*a.k.a.* one season) densities and frequencies of each species were determined using flow cytometry and a fixed volume sample (3.3%) of the community was transferred to a new 96-well plate containing fresh media, marking the beginning of a new season (Supporting Materials and Methods).

Applying single-species logic to this community, the resistant species, *C. glabrata*, should dominate in the presence of enough drug. Indeed, there is evidence this is predictive of clinical outcomes: the use of fluconazole prophylaxis was found to influence the proportion of *C. albicans* and *C. glabrata* isolated from the blood of patients with candidemia (*37*), leading to an increase in *C. glabrata* frequency. Fluconazole withdrawal should then shift the community towards the sensitive species, *C. albicans*. Importantly, we can replicate both these observations using our community: under fluconazole treatment the drug resistant *C. glabrata* dominates and when the drug is removed, the sensitive *C. albicans* subsequently recovers. This creates a repeatable, cyclical dynamic as the drug is repeatedly applied and withdrawn (Figure 1(a)).

But is this the only dynamic possible following fluzonazole withdrawal? To answer this we now systematically explore community dynamics under different abiotic conditions by applying ideas from microbial population biology (*38*). Recalling *C. albicans* are inoculated into the microcosm at proportion f, suppose F denotes the frequency of *C. albicans* after one season, so $R(f) = F/f$ denotes the change in *C. albicans* relative frequency. Now, $F = f \cdot R(f)$ is a 'single-season frequency change map' that gives the frequency of *C. albicans* after one season and we will write F as a mathematical function, calling it Φ, thus $\Phi(f) = f \cdot R(f)$. Repeated applications of Φ to frequency values can therefore be used to determine the *C. albicans* frequency after any number, $n \geq 1$, of seasons, provided a given initial (inoculum) frequency f_0 is known. So, $f_1 = \Phi(f_0)$ is the frequency

of *C. albicans* after one season, $f_2 = \Phi(\Phi(f_0)) = \Phi(f_1)$ is the frequency of *C. albicans* after two seasons, $f_3 = \Phi(\Phi(\Phi(f_0))) = \Phi(f_2)$, and so on. In population dynamics theory it is common to write season number as a subscript n, so $f_{n+1} = \Phi(f_n)$ is a shorthand representation of the season-by-season dynamics at season n. It follows by definition that $\Phi(0) = 0$ because with no *C. albicans* in the inoculum, it cannot appear subsequently. Similarly, $\Phi(1) = 1$ must hold as a closed community containing only *C. glabrata* initially must always do so (see Supplementary Information §2 for details).

What should a biologically reasonable Φ look like? Figure 1(b) shows four lab-derived exemplars and we also use a bottom-up mathematical model that builds theoretical Φ functions (Figure 1(c), Supplementary Information §3). The latter can incorporate many microbial life history traits and environmental variables but here we focus on antimicrobials (at concentration a) and extracellular nutrient concentrations, say g denoting the carbon source glucose. We restrict attention for now to just a, ignoring g dependence, and write $\Phi(f, a)$ to emphasise this.

We now ask how the community responds to an antimicrobial by introducing a sequence of antimicrobial dosages, a_n, so that $f_{n+1} = \Phi(f_n, a_n)$ where the treatment can change with each season. In the clinic, a_n might be one of two extremes, either a high dosage above the drug's MIC (minimal inhibitory concentration) or zero when treatment stops. Figure 1(c) shows two theoretically-constructed Φ functions, Φ_{on} and Φ_{off}, motivated by this clinical context:

$$f_{n+1} = \begin{cases} \Phi_{\text{on}}(f_n) & : \text{ if antimicrobial is applied (so } a_n \geq \text{MIC)}, \\ \Phi_{\text{off}}(f_n) & : \text{ if antimicrobial is not applied (so } a_n = 0). \end{cases}$$

Empirical Φ functions (Figure 1(b)) strongly resemble their theoretical counterparts (Figure 1(c)) and, in these figures, both theory and data exhibit reversible resistance.

However, theory-derived Φ_{on} and Φ_{off} provide information about when not to expect reversible resistance (Figure 2(a-d)) and the shape of these two functions is all-important. If Φ_{on} satisfies $\Phi_{\text{on}}(f) < f$ for all f between 0 and 1, then $f_{n+1} = \Phi_{\text{on}}(f_n) < f_n$ follows, meaning the frequency of *C. albicans* decreases each season when drug is applied (Figure 2(a)). Conversely, if $\Phi_{\text{off}}(f) > f$ for all f then *C. albicans* increases each season after treatment withdrawal, whence resistance is reversible (Figure 2(b)). Points of separation, or separatrixes, between these two cases arise when there are frequencies, f, for which $\Phi_{\text{off}}(f) = f$ (Figure 2(c,d)). As a consequence, for our purposes a tipping point, f_u, satisfies $\Phi_{\text{off}}(f_u) = f_u$ and other technicalities (Supplementary Information §2

and §4) . This condition allows either *C. albicans* or *C. glabrata* to dominate in the absence of drug and, as a result, drug treatment can coerce the microcosm towards either possibility when treatment stops (Supplementary Information §4).

Using a fixed-glucose stochastic model $f_{n+1} = \Phi(f_n, a_n) + \sigma_n$, where σ_n is small-variance noise and the form of Φ is defined in Supplementary Information §3, we show that resistance need not be reversible because a tipping point is encountered in a theoretical 4-day treatment (Figure 2(f-g)) that is not encountered if treatment terminates at 3 days (Figure 2(e)). Figure 2(h,i) then incorporates glucose dependence, g, and explores a model $\Phi(f, a, g)$ in different abiotic conditions by systematically varying g and antibiotic dose, a (Supplementary Information §3.2 and §4). This is impossible to do in empirical microbial ecologies but computational simulations (Figure 2(h)) show the dominant *Candida* species, *albicans* or *glabrata* or neither, in the (a, g)-plane (this is the 'dose-response mosaic'). This computational analysis shows the dosage at which tipping occurs depends on glucose availability and we will therefore now also manipulate glucose availability in our empirical microcosm.

So does the laboratory treatment community also possess tipping points when antibiotic dose or else glucose availability vary? This is difficult to assess directly for several reasons. First, our modelling framework is general but simple and so is not able to accurately pinpoint tipping points in an empirical context. Second, theoretical tipping mechanisms require an unstable fixed point (f_u) under drug-free conditions. These are hard to identify empirically because observations move away from unstable fixed points and so these points, if present, cannot be detected directly in longitudinal data, we can only infer their presence. Other warning signals of tipping exist (*39, 40*) for example so-called 'critical slowing down' (*41, 42*), slow recovery from perturbations (*43, 44*), an increase in autocorrelation (*45*), an increase in the variation of fluctuations (*46, 47*) or timeseries skewness (*48*). We therefore chose variance increases because modelling indicates between-replicate variance (BRV) should increase sharply at a tipping point (Figure 3).

We sought antibiotic tipping experimentally for three treatments, α, β and γ that are designed to explore the dose response mosaic as fully as possible. First, α) glucose is held constant but the drug steadily withdrawn; β) glucose and drug are held constant and γ) glucose is reduced while the drug is withdrawn (Figure 4(a)). For these treatments, glucose varied between $0.1 - 4\%$ mirroring prior *in vitro Candida* experiments (*49, 50*) and fluconazole varied between $0 - 3\mu$g/ml, mirroring

prior *in vitro* drug-adaptation studies (*51*).

Treatments α and β lead to reversible resistance (Figure 4(b)) whereby the *C. albicans* frequencies on the last season have almost unimodally distributed between-replicate variation (BRV) (Figure 4(c)). However, treatment γ exhibits characteristics of tipping: BRV statistics of *C. albicans* frequencies on the last observed season approximate a uniform distribution (Figure 4(c)) and mean BRV spikes on season 6 (approximately $8\times$ increase, Figure 4(d,e)). The rapid divergence of replicate trajectories (Figures 4(b), S12) that forms a uniform distribution of treatment outcomes for γ (Figure 4(c)) in a manner consistent with theory (Figure S9) means that many community trajectories have not returned to their inoculum positions, in contrast to reversible resistance (Figure 1(a)) where they have.

Discussion

The reversibility of resistance is often conceptualised through resistance costs (*16*), a property which ensures resistance genes are lost following drug withdrawal due to a fitness reduction of the mutants that carry them. However the analogy of resistance costs between species is difficult to define. For example, without the drug in our community the *Candida* species have different metabolism (*67*) from which complex, density and frequency dependent ecological interactions like cheating and cooperation can result (*53*). Indeed, the myriad ecological interactions present in natural communities are necessarily perturbed by an antibiotic drug so a model of resistance progression in which resistant and susceptible microbes differ by a single allele will have limited explanatory power here. Thus we invoke tipping as a new mechanism for understanding the dynamics of drug resistance following exposure to antibiotics.

The explanation behind the tipping-induced irreversibility of resistance is this: if a community could persist in multiple configurations in the absence of drug (*17*), antibiotics, indeed, any abiotic perturbation, might push the community into the 'basin of attraction' of the most resistant configuration from all those available. So even if treatment stops, resistance species' frequencies could increase. Our mathematical models illustrate just two basins of attraction, one above the tipping point and one below (Figure 3(a)) but real-world communities may well have more.

Unfortunately, the key ingredient for tipping, multi-stability, is known to be difficult to demonstrate in real communities (*17*) but if present, we then know the removal of drug can create an

uncertain future for that community. Figure 3(b) and 4(b) show in theory and in data how some of those divergent futures pan out; some return whence they came, others move towards a new configuration of the community. This is the defining property of multistability (*17*) and if this new configuration comprises more species that are less susceptible to the drug than were there prior to treatment, resistance in the community will increase even though treatment has stopped.

Our microcosms highlight just one treatment consistent with this theory (Figure 4) but what other treatments might do this? Indeed, data show that not all drug treatments induce tipping (Figure 4). However, mathematics answers the question: any co-variation of abiotic environment and drug, whether stochastic, cyclical, gradual or abrupt that guides the community into a region of the dose-response mosaic that exhibits multi-stability (Figure 2(h) grey zone) creates the right conditions for tipping. Our empirical data provides one example of this (treatment γ) from the infinitely many treatments we could have tested and the mathematical model we present undergoes tipping with this type of treatment (Figure S9) and for many more besides. The theoretical treatment examples we provide (Figure 3 and S10) illustrate, perhaps, the simplest possible abiotic variation that can exhibit tipping, namely the abrupt cessation of a constant-dose drug treatment (Figure 3) of the kind given to patients in the community.

To conclude, we argue that single-species logic is insufficient to understand resistance in microbial communities. Particularly lacking is a theory of how abiotic variation promotes resistance and yet this is relevant to patients. For example, infections involving *C. glabrata* are more frequently found in diabetic patients with high blood glucose levels than in patients with lower glucose levels (*54, 55*), indicating that nutrient availability may play a role in clinical resistance, just as it does in our community. Our observations may also indicate potential for alternative therapeutic rationales for polymicrobial infections. Diet is known to alter the host microbiota (*56–58*) and so fashioning specific environments by manipulating nutrients might tip the balance of competition in favour of drug-susceptible species and render an infection more amenable to treatment. There is a precedence for this idea (*59–61*).

Acknowledgements

In memory of our friend and colleague Ken Haynes who sadly passed away on 19th March 2018.

References

1. D. J. Payne, M. N. Gwynn, D. J. Holmes, D. L. Pompliano, *Nat Rev Drug Discov* **6**, 29 (2007).

2. P. M. Mira, *et al.*, *PLoS ONE* **10**, 1 (2015).

3. M. H. Kollef, *Clin.Infect.Dis.* **43 Suppl 2**, S82 (2006).

4. M. Sundqvist, *Upsala journal of medical sciences* **119**, 142 (2014).

5. J. Lee, *et al.*, *Journal of Antimicrobial Chemotherapy* **60**, 629 (2007).

6. J. J. Rahal, *et al.*, *Jama* **280**, 1233 (1998).

7. P. P. Cook, P. G. Catrou, J. D. Christie, P. D. Young, R. E. Polk, *Journal of Antimicrobial Chemotherapy* **53**, 853 (2004).

8. S. Nijssen, *et al.*, *Intensive Care Medicine* **36**, 512 (2010).

9. Y. Chong, *et al.*, *PLoS ONE* **8** (2013).

10. Y. Takesue, *et al.*, *Journal of Hospital Infection* **75**, 28 (2010).

11. S. Hashino, *et al.*, *European Journal of Clinical Microbiology and Infectious Diseases* **31**, 173 (2012).

12. S. Sarraf-Yazdi, *et al.*, *Journal of Surgical Research* **176**, e73 (2012).

13. F. Gruson, Didier; Gilles, Hilbert; Vargas, *American Journal of Respiratory and Critical Care Medicine* **162**, 837 (2000).

14. H. J. Van Loon, *et al.*, *American Journal of Respiratory and Critical Care Medicine* **171**, 480 (2004).

15. D. Warren, *et al.*, *Crit Care Med* **32**, 2450 (2004).

16. D. I. Andersson, D. Hughes, *Nat Rev Microbiol* **8**, 260 (2010).

17. D. Gonze, L. Lahti, J. Raes, K. Faust, *ISME J* **11**, 2159 (2017).

18. S. Panda, *et al.*, *PLoS ONE* **9** (2014).

19. H. E. Jakobsson, *et al.*, *PLoS ONE* **5** (2010).

20. L. Dethlefsen, M. McFall-Ngai, D. a. Relman, *Nature* **449**, 811 (2007).

21. D. A. Antonopoulos, *et al.*, *Infection and Immunity* **77**, 2367 (2009).

22. A. E. Perez-Cobas, *et al.*, *Gut* **62**, 1591 (2013).

23. L. Dethlefsen, D. A. Relman, *Proc Natl Acad Sci U S A* **108 Suppl**, 4554 (2011).

24. L. V. McFarland, G. W. Elmer, C. M. Surawicz, *Am J Gastroenterol* **97**, 1769 (2002).

25. L. Cousin, M. L. Berre, V. Launay-Vacher, H. Izzedine, G. Deray, *Nephrol Dial Transplant* **18**, 2227 (2003).

26. H. R. Ashbee, *et al.*, *J Antimicrob Chemother* **69**, 1162 (2014).

27. T. C. Havey, R. A. Fowler, R. Pinto, M. Elligsen, N. Daneman, *Can J Infect Dis Med Microbiol* **24**, 129 (2013).

28. S. L. Cowart, M. E. Stachura, *Glucosuria* (Butterworth Publishers, a division of Reed Publishing, 1990).

29. A. P. C. P. Carlotti, *et al.*, *QJM* **100**, 125 (2007).

30. G. Manoj, M. R. George, R. Dipu, J. Jishnu **8**, 60 (2017).

31. K. m. Ho, T. s. Cheng, *Medical Bulletin* **15**, 23 (2010).

32. R. P. Wenzel, C. Gennings, *Clinical Infectious Diseases* **41 Suppl 6**, S389 (2005).

33. G. D. Brown, *et al.*, *Sci Transl Med* **4**, 165rv13 (2012).

34. D. H. Kett, E. Azoulay, P. M. Echeverria, J.-L. Vincent, *Crit Care Med* **39**, 665 (2011).

35. P. G. Pappas, *et al.*, *Clinical infectious diseases : an official publication of the Infectious Diseases Society of America* **38**, 161 (2004).

36. J. H. Rex, *et al.*, *Clin Infect Dis* **24**, 235 (1997).

37. O. Lortholary, *et al.*, *Antimicrob Agents Chemother* **55**, 532 (2011).

38. M. E. Hibbing, C. Fuqua, M. R. Parsek, S. B. Peterson, *Nat Rev Microbiol* **8**, 15 (2010).

39. M. Scheffer, S. Carpenter, J. a. Foley, C. Folke, B. Walker, *Nature* **413**, 591 (2001).

40. T. M. Lenton, *et al.*, *Proceedings of the National Academy of Sciences* **105**, 1786 (2008).

41. C. Wissel, *Oecologia* **65**, 101 (1984).

42. K. Wiesenfeld, B. Mcnamara, *Physical Review A* **33**, 629 (1986).

43. L. Dai, D. Vorselen, K. S. Korolev, J. Gore, *Science* **336**, 1175 (2012).

44. M. Scheffer, *et al.*, *Nature* **461**, 53 (2009).

45. V. Dakos, *et al.*, *Proceedings of the National Academy of Sciences of the United States of America* **105**, 14308 (2008).

46. T. M. Lenton, *Nature Climate Change* **1**, 201 (2011).

47. S. R. Carpenter, W. A. Brock, *Ecology Letters* **9**, 308 (2006).

48. V. Guttal, C. Jayaprakash, *Ecology Letters* **11**, 450 (2008).

49. G. S. Baillie, L. J. Douglas, *Antimicrob Agents Chemother* **42**, 1900 (1998).

50. N. J. Basson, *J Med Microbiol* **49**, 969 (2000).

51. M. Huang, M. McClellan, J. Berman, K. C. Kao, *Eukaryot Cell* **10**, 1413 (2011).

52. I. V. Ene, S. Brunke, A. J. P. Brown, B. Hube, *Cold Spring Harb Perspect Med* **4**, a019695 (2014).

53. R. C. MacLean, I. Gudelj, *Nature* **441**, 498 (2006).

54. P. L. Fidel Jr., J. A. Vazquez, J. D. Sobel, *Clinical Microbiology Reviews* **12**, 80 (1999).

55. D. Ray, *et al.*, *Diabetes Care* **30**, 312 (2007).

56. E. D. Sonnenburg, *et al.*, *Cell* **141**, 1241 (2010).

57. L. A. David, *et al.*, *Nature* **505**, 559 (2014).

58. B. U. Metzler-Zebeli, J. C. Lange, R. T. Zijlstra, M. G. Gänzle, *Livestock Science* **152**, 31 (2013).

59. K. R. Allison, M. P. Brynildsen, J. J. Collins, *Nature* **473**, 216 (2011).

60. B. Peng, *et al.*, *Cell Metab* **21**, 249 (2015).

61. M. Zampieri, *et al.*, *Molecular Systems Biology* **13**, 917 (2017).

62. Z. I. Botev, J. F. Grotowski, D. P. Kroese, *Ann. Statist.* **38**, 2916 (2010).

63. R. E. Beardmore, I. Gudelj, D. A. Lipson, L. D. Hurst, *Nature* **472**, 342 (2011).

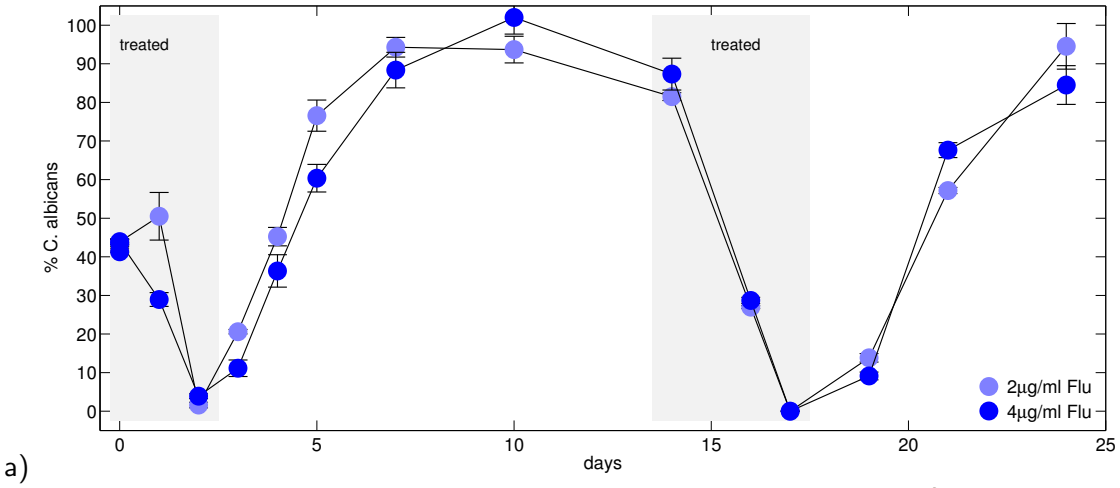
treated
treated
% C. albicans
days
2µg/ml Flu
4µg/ml Flu

a)

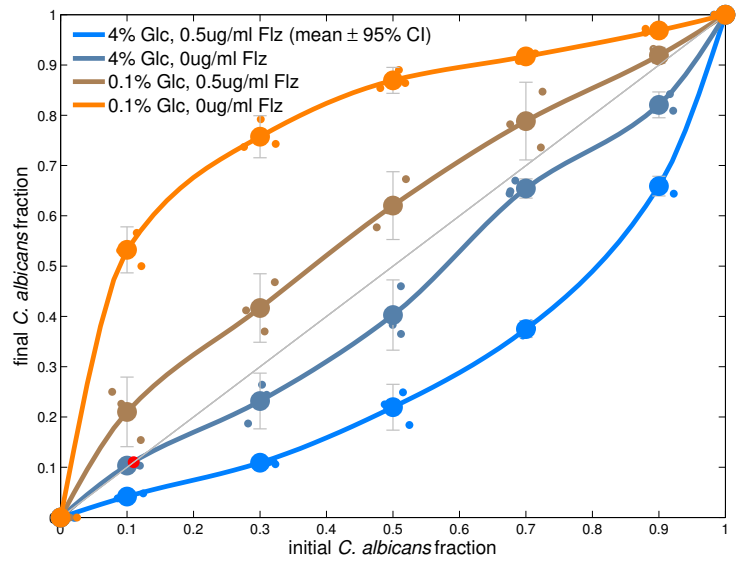
4% Glc, 0.5ug/ml Flz (mean ± 95% CI)
4% Glc, 0ug/ml Flz
0.1% Glc, 0.5ug/ml Flz
0.1% Glc, 0ug/ml Flz
final C. albicans fraction
initial C. albicans fraction

b)

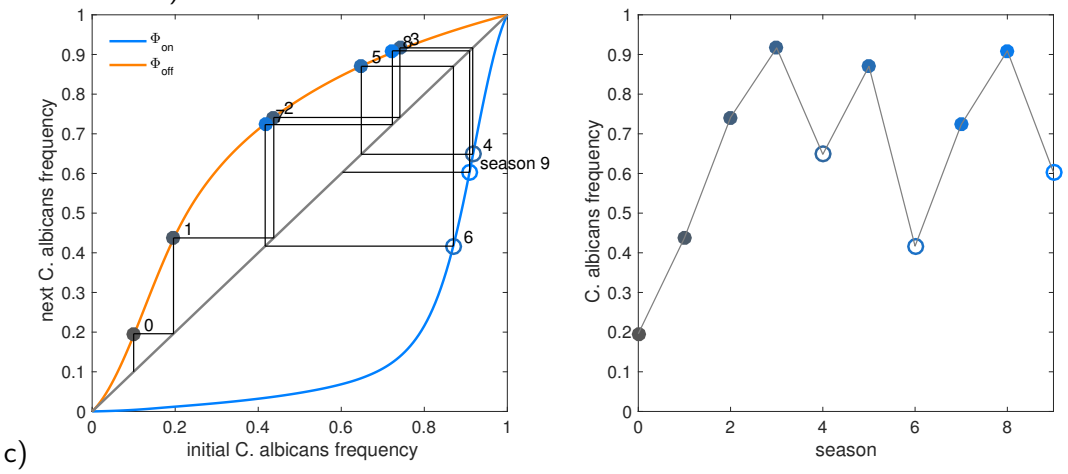
Φon
Φoff
next C. albicans frequency
initial C. albicans frequency
season 9
C. albicans frequency
season

c)

Figure 1: a) Lab data: *C. albicans* and *C. glabrata* are inoculated at 50-50 proportions into growth in SC media supplemented with 0.1% glucose and propagated in the presence of fluconazole for 2 seasons, the *C. albicans* frequency subsequently decreases. After 2 seasons, fluconazole is withdrawn and *C. albicans* recovers. When fluconazole is later re-applied for 3 seasons *C. albicans* again decreases in frequency, and so the cycle repeats. (Grey boxes mark seasons undergoing fluconazole treatment, error bars are mean $\pm$ 95% CI, $n = 3$, raw data shown.) b) Lab data: the initial *C. albicans* frequency (f) on the x-axis versus the final frequency each season obtained using the laboratory microcosm on the y-axis, aka $\Phi(f)$ (four exemplars are shown; error bars are mean $\pm$ 95% CI, $n = 3$; glucose and fluconazole given in the legend, SC denotes synthetic complete media). c) Theoretical example: how to read $\Phi(f)$ to understand dynamics: starting at timepoint 0, the dynamics follow Φ_{on} while treatment proceeds, it then follows Φ_{off} when treatment stops. The sequence of treatments here is (on,on,on,on,off,on,off,on,on,off). The right plot shows how *C. albicans* reversibly increases and decreases in frequency according to whether drug is used (solid dot) or not (open circle).

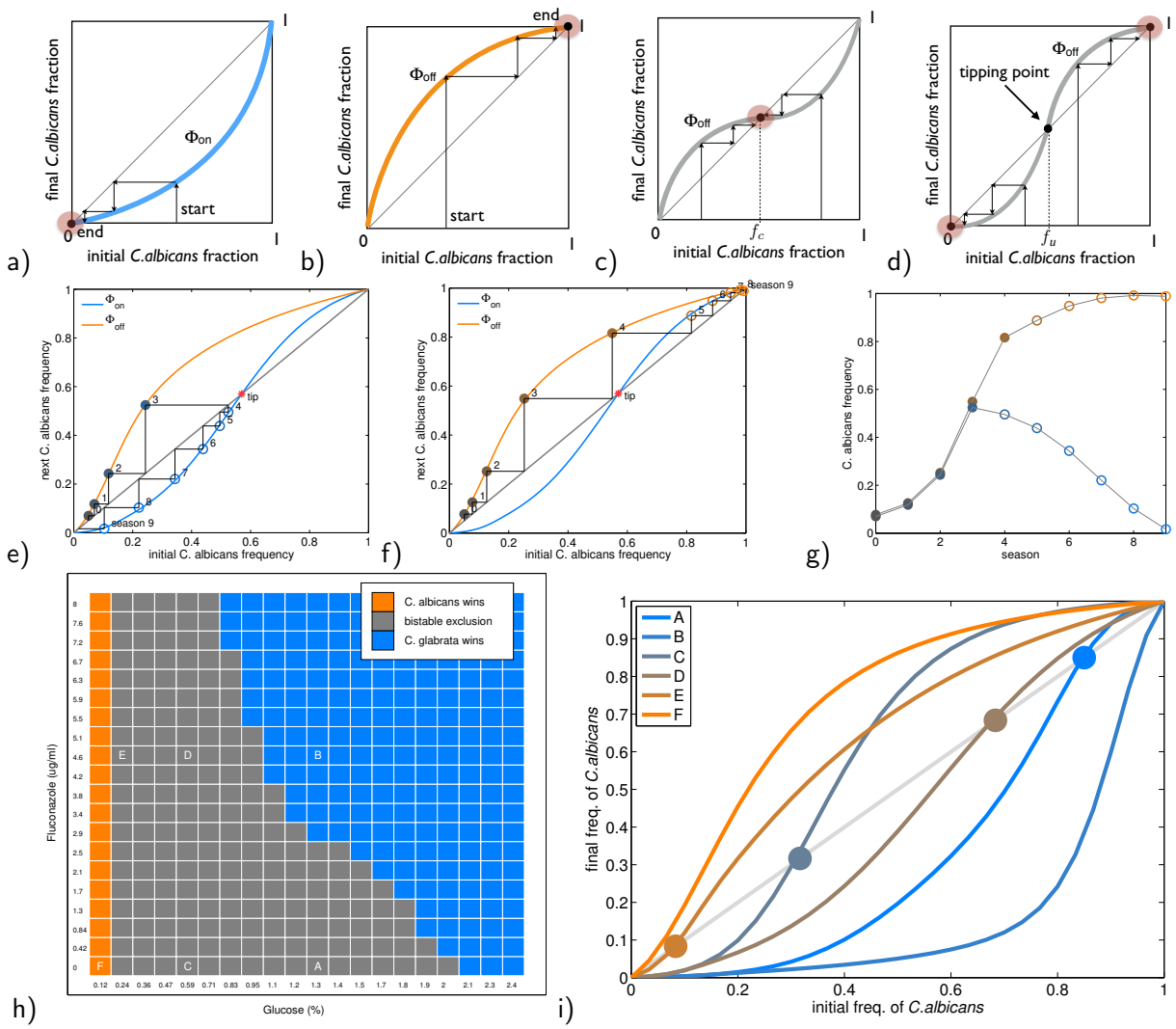
a)
final C.albicans fraction
initial C.albicans fraction
Φon
start
end
b)
Φoff
start
end
c)
Φoff
$\hat{f}_c$
d)
Φoff
tipping point
$\hat{f}_u$
e)
Φon
Φoff
next C. albicans frequency
initial C. albicans frequency
tip
season 9
f)
season 9
g)
C. albicans frequency
season
h)
C. albicans wins
bistable exclusion
C. glabrata wins
Fluconazole (μg/ml)
Glucose (%)
i)
A
B
C
D
E
F
final freq. of C.albicans
initial freq. of C.albicans

Figure 2: Population dynamics theory states that one can deduce multi-season frequency dynamics from the 'cobweb diagram' determined from the initial *C. albicans* frequency plotted versus the final frequency each season. a): $\Phi_{\rm on}$ lies below the diagonal so *C. glabrata* outcompetes *C. albicans*. b) $\Phi_{\rm off}$ lies above the diagonal line of equal frequencies, so *C. albicans* outcompetes *C. glabrata*. c) $\Phi_{\rm off}$ is such that there exist a special frequency, f_c, which lies on the diagonal line and $\Phi_{\rm off}(f) > f$ for $0 < f < f_c$ while $\Phi_{\rm off}(f) < f$ for $f_c < f < 1$, this is a stable coexistence state. d) $\Phi_{\rm off}$ is such that there exist a special frequency, f_u, which lies on the diagonal line and $\Phi_{\rm off}(f) < f$ for $0 < f < f_u$ while $\Phi_{\rm off}(f) > f$ for $f_u < f < 1$. In this case either species can dominate depending on their initial frequencies: if the initial frequency of *C. albicans* is smaller than f_u then *C. albicans* loses out in competition to *C. glabrata*, otherwise *C. glabrata* loses out; this is 'bistable exclusion'. e) A theoretical example of a 3-season treatment, which stops short of the tipping point (marked 'tip') with seasons 4-9 continuing without the drug being applied. f) A theoretical example of a 4-season treatment which goes beyond the tipping point, causing the divergence in trajectories following drug withdrawal cause by the tipping point as shown in (g). h) This is a theoretical two-dimensional *dose-response mosaic*, it describes the equilibrium outcome of competition in the *Candida* community as glucose and fluconazole are varied. *C. albicans* wins the competition inside orange squares, *C. glabrata* wins inside the blue squares and bistable exclusion occurs in the grey squares. Drug on-off treatments that encounter the latter may exhibit tipping (e.g. ABAB, FEFE and CDCD treatment sequences), treatments that stay inside the former will exhibit reversible resistance (e.g. an FBFB sequence). i) theoretical Φ functions at points A-F in the dose response mosaic, with dots highlighting the location of the special frequency f_u for each Φ that crosses the diagonal.

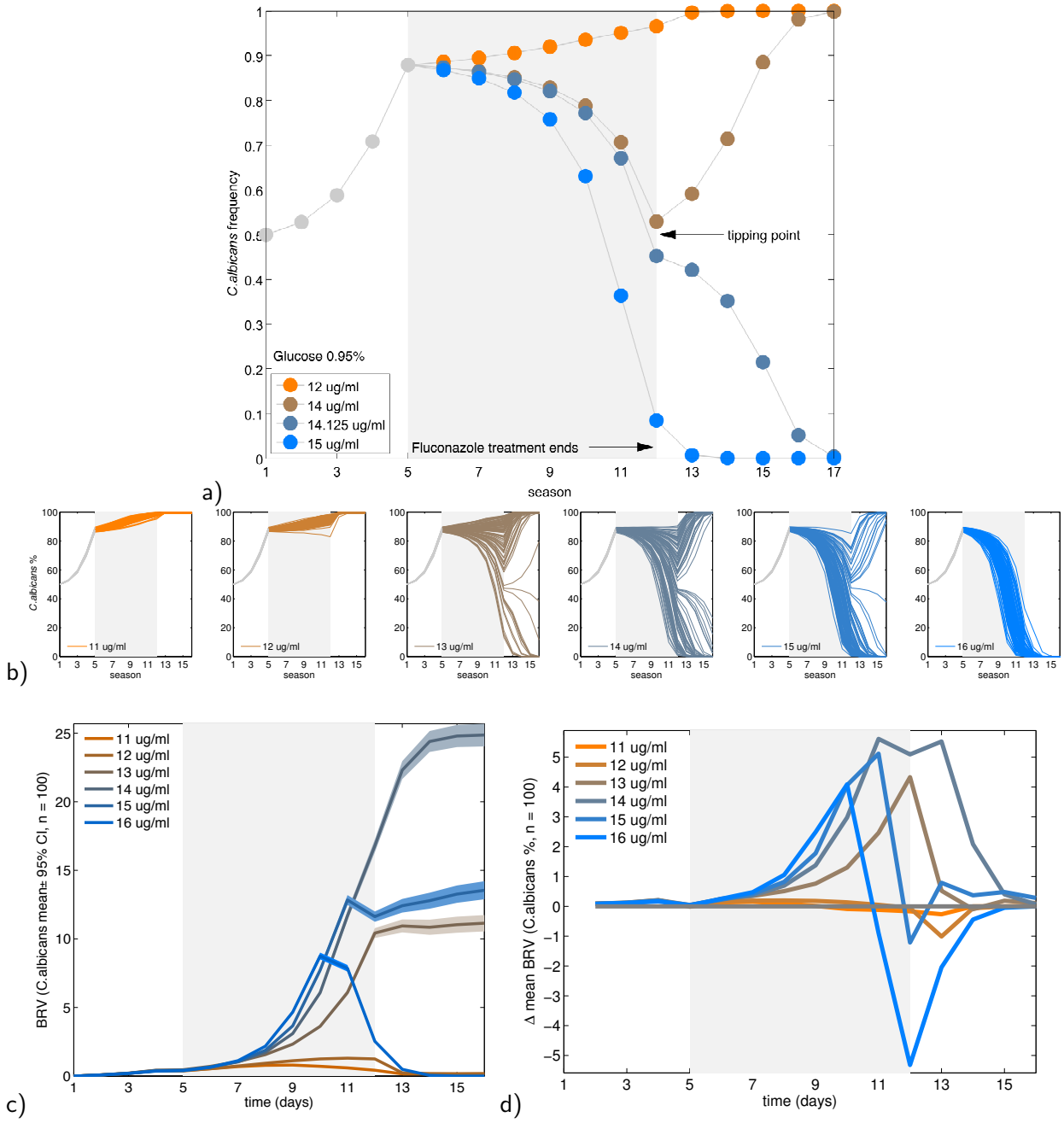
a)
C.albicans frequency
season
Glucose 0.95%
12 ug/ml
14 ug/ml
14.125 ug/ml
15 ug/ml
tipping point
Fluconazole treatment ends
b)
C.albicans %
11 ug/ml
12 ug/ml
13 ug/ml
14 ug/ml
15 ug/ml
16 ug/ml
c)
BRV (C.albicans mean± 95% CI, n = 100)
time (days)
d)
Δ mean BRV (C.albicans %, n = 100)
time (days)

Figure 3: The dose-response mosaic shows tipping points are encountered in many ways, for example by varying glucose concentration (see Supporting Fig. S10 for details) or as fluconazole concentration is varied (a). In (a) four, fixed-dose treatments start on season 5 and end on season 12 (grey box) at a 0.95% (by volume) glucose dose. First, the community converges towards *C. albicans* domination in the absence of drug (orange dots). *C. glabrata* starts to dominate as drug is applied, but it rescinds when treatment ends (brown dots) and the community returns to its pre-treatment composition and then continues towards *C. albicans* dominance with more seasons. However, a tipping point appears at just high-enough fluconazole dose (dark blue dots) whereby the post-treatment trajectory diverges from the previous outcome (at a slightly lower drug dose) and *C. albicans* is lost as the seasons pass. Royal blue dots show trajectories at dosages well above the tipping point. (b) Introducing additive stochastic noise to simulations from (a) shows that replicate trajectories diverge at the tipping point, creating large variations between frequency trajectories that had identical drug dosage regimes and initial *Candida* frequencies. A signature we can seek in empirical data: between replicate variation (BRV) spikes at the tipping point (c), causing a large season-by-season change in BRV (ΔBRV here taken to be the mean change in standard deviation) that is significantly positive at the tipping point (d).

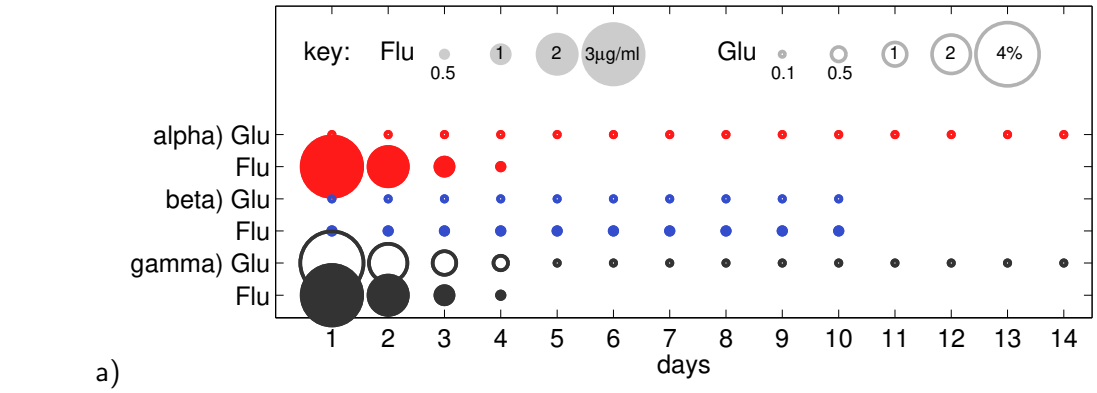
key: Flu 0.5 1 2 3µg/ml Glu 0.1 0.5 1 2 4%
alpha) Glu
Flu
beta) Glu
Flu
gamma) Glu
Flu
1 2 3 4 5 6 7 8 9 10 11 12 13 14
days

a)

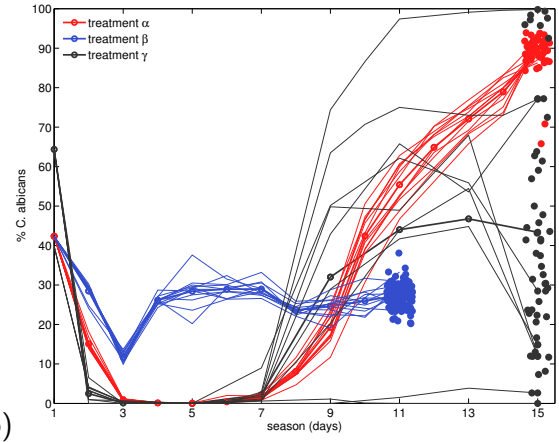
treatment α
treatment β
treatment γ
% C. albicans
season (days)

b)

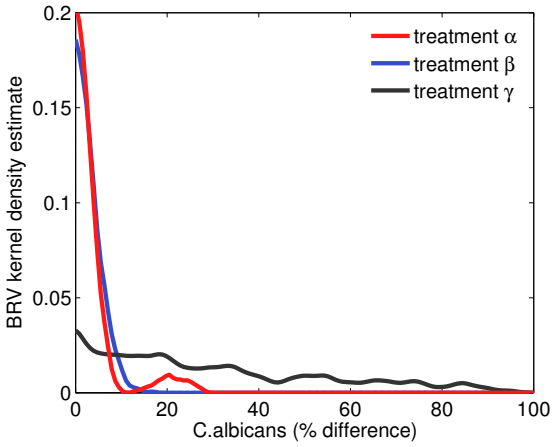
treatment α
treatment β
treatment γ
BRV kernel density estimate
C.albicans (% difference)

c)

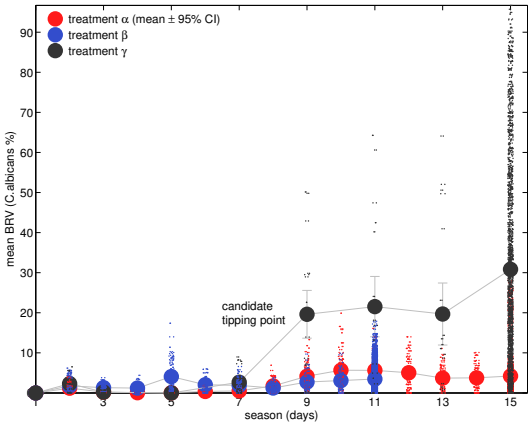
treatment α (mean ± 95% CI)
treatment β
treatment γ
mean BRV (C.albicans %)
candidate tipping point
season (days)

d)

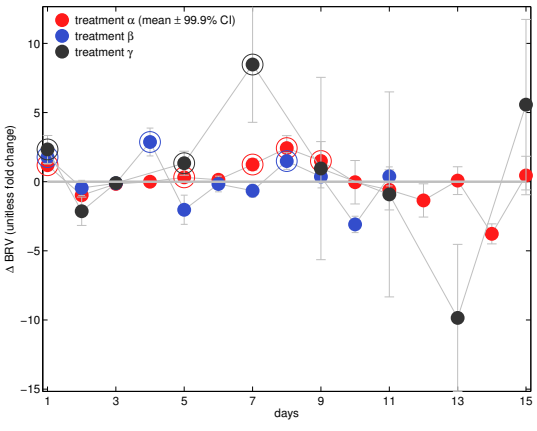
treatment α (mean ± 99.9% CI)
treatment β
treatment γ
Δ BRV (unitless fold change)
days

e)

Figure 4: a) Three laboratory treatments with different dynamics: treatments α (red) and γ (black) withdraw fluconazole but β (blue) keeps it at constant levels (dosages represented as circle sizes). The laboratory experimental trajectories of treatments are shown in (b) and the corresponding between-replicate variation (BRV) is shown in (c) as indicated by the kernel density estimate of the distribution of final-season *C. albicans* frequency differences (48 replicates for α, 96 for β and 55 for γ). The trajectories of treatments α and β have low BRV in species frequencies at all times whereas γ has high BRV at the end of treatment. The trajectories show why: community dynamics for β maintain steady-state and *C.albicans* sweeps through the community during treatment α following drug withdrawal. However, in γ trajectories of different replicates vary markedly beyond season 6 whereby either species can dominate by season 14, despite all replicates having close to 50-50 initial composition (Supporting Fig. S11 has additional data). d) Data from the *Candida* community shows mean BRV increases significantly, approximately 8-fold for treatment γ on season 6. Treatments α and β also have significant increases on occasion, but by no more than 3-fold. Taking a conservative Bonferroni-corrected significance at the level $p < 0.001$ in an F-test using linear regression (see Methods), significant changes in mean BRV are shown in (e) as circled dots. The largest increase (approximately 8-fold) is significant and occurs in treatment γ on season 7 (error bars explained in legend).

Methods

Numerical simulations of a theoretical community model were obtained using Matlab's differential equation solvers to generate the season-by-season dynamical map $\Phi(f)$. Differential equations were parameterised using data from *C. albicans* and *C. glabrata*, as detailed in the supplementary.

To determine tipping points, we sought significant increases in between-replicated variation (BRV) defined as follows. If $\mathcal{F} = \{f_j\}_{j=1}^{n}$ is the set of observed *C. albicans* frequencies, expressed as values between zero and one (although some figures express this as a percentage), the set of between-replicate differences is then $\{|f_j - f_k|\}_{j,k=1,j>k}^{n}$ and mean BRV is the mean of this set; note, this is one form of set radius. As the frequency of *C. glabrata* is $G_j = 1-f_j$ and $G_j - G_k = 1-f_j-(1-f_k) = f_k - f_j$, *C. glabrata* frequency data has the same between-replicate differences as *C.albicans*.

Kernel density estimates were obtained for distributions of BRV values (Figure 4(a)) using a kernel estimation algorithm implemented in Matlab (*62*). To test for significant season-by-season differences in BRV, BRV_n and BRV_{n+1} observed at seasons n and $n+1$, we applied linear regression to test (with $p < 0.001$) against the null hypothesis of a constant mean BRV between those seasons, testing for a non-zero slope parameter from the regression. This is written ΔBRV and this change was found to be largest for season 6 of treatment γ (Figure 4(b)).

Experimental methods

Full experimental methods are given in the supplementary text.

Data availability statement

Data files and computer codes will be provided prior to publication.

Supporting Material

Contents

1 Materials and Methods

1.1 Strains and assay medium

The strains *Candida albicans* ACT1-GFP and *Candida glabrata* ATCC2001 were used throughout this paper in all Experimental designs $1-3$. The strain *C. albicans* ACT1-GFP strain is SBC153 (*64*) with pACT1-FLAG-GFP integrated at the ACT1 locus by means of positive selections using a nourseothricin resistance cassette. The strain *C. glabrata* ATCC2001 is the wild type reference strain obtained from the American Type Culture Collection. The assay medium throughout was synthetic complete (SC) (0.67% w/v yeast nitrogen base without amino acids, 0.079% w/v synthetic complete supplement mixture (Formedium, Hunstanton, UK)).

1.2 Measuring growth of *C. albicans* and *C. glabrata* in isolation in the absence / presence of drugs

Overnight cultures in YPD of C. albicans and C. glabrata were diluted, counted on hemocytometer, and adjusted to 2×10^7 cells/mL in SC medium containing 2% (weight/volume) glucose. Sterile plastic microdilution plates containing 96 flat-bottomed wells were utilized. Stock solution of fluconazole was diluted in SC medium and dispensed in $75\,\mu$L volumes into six replicate wells to yield nine two-fold serial dilutions of fluconazole with final concentrations ranging between $0-64\,\mu$g/mL. For each drug concentration, three of the six replicate wells were filled with additional $75\,\mu$L from the *C. albicans* strain suspension while the remaining three wells were filled with $75\,\mu$L from the *C. glabrata* strain suspension. The plate was sealed with a transparent adhesive seal and two holes were punctured over each well by means of a sterile needle. The plate was incubated at 30^oC with shaking over 24 hours and growth monitored by measuring the absorbance of the cell suspensions at 650 nm (A_{650}). Absorbance units were converted into number of cells per ml by means of calibration curves prepared for each *Candida* species.

1.3 Drug susceptibility dose-response for *C. albicans* and *C. glabrata*

Standard micro-dilution susceptibility testing was performed in sterile 96-well flat-bottom microtiter plates with the following modifications. Fluconazole was diluted from a 2mg/mL stock solution to a dilution series ranging from 512 to $0\,\mu$g/mL in SC media containing 1% or 4% glucose (weight/volume), at a volume of $75\,\mu$L per well. Overnight cultures in YPD of *C. glabrata* and *C. albicans* were counted by haemocytometer and diluted to 10^5 cells/mL in SC broth containing either 1% or 4% glucose. For each species, $75\,\mu$L of cell suspension was added per well, resulting in a final volume of $150\,\mu$L which contained 5×10^4 cells, a final drug concentration of $256, 192, 128, 96, 64, 48, 32, 16, 8, 4, 2$ or $0\,\mu$g/mL of fluconazole and either 1% or 4% glucose. The plate was sealed with a transparent adhesive seal and two holes were punctured over each well, by means of a sterile needle, for aeration. Plates were incubated for 48 hours at 30^oC after which final absorbance was measured at A_{595}. All samples were assayed in technical triplicate.

1.4 Competition of *C. albicans* and *C. glabrata* in the absence/presence of drugs

Overnight cultures in YPD of *C. albicans* and *C. glabrata* were diluted, counted on hemocytometer, and adjusted to 2×10^7 cells/mL in SC medium containing either 0.1, 2, or 4% (weight/volume) glucose. The two *Candida* species were then mixed to achieve a range of starting ratios ($0, 10, 30, 50, 70, 90$

and 100% *C. albicans*) The cell suspension was then diluted 1:1 in SC media containing two times desired fluconazole concentration (0, 0.5, or $2\,\mu g/mL$) to a final volume of $150\,\mu L$ in a 96 well flat bottom microtiter plate. Plates were sealed using sterile adhesive films, two holes were punched in seal above each well using a sterile needle, and incubated overnight in orbital shaker set at 30^oC, 180 rpm. Each condition was repeated in triplicate. After 24 hour incubation period (one season) plates were opened, the contents of the well were vigorously pipetted to achieve a homogenous cell suspension, and relative frequency of *C. albicans* ACT1-GFP was determined by flow cytometry in the following way (Supporting Fig. S1). Cellular fluorescence from GFP was determined quantitatively with a FACSAria flow cytometer (Becton Dickinson, CA, USA) equipped with a 20mW, 488 nm argon ion laser. All samples were suspended in phosphate buffered saline (PBS) and briefly sonicated to disperse potential cell clumps prior to analysis. Typically, 10000 cells were analysed per competition sample with the following settings: forward scatter (150 V, log mode) and side scatter (200 V, log mode). GFP was detected on a $530/30$ filter (600 V, log mode) and sample acquisition was performed using BD FACSDiva software. Initially, a sample consisting of *C. albicans* ACT1-GFP cells only was detected and gated to contain $99 - 100\%$ of all measured events as positive for GFP fluorescence. All events occurring within the gate during subsequent analysis of competition samples were considered to be *C. albicans* ACT1-GFP cells. For any given competition sample, the frequency of gated events was calculated by means of FlowJo software and was taken to be the population percentage of *C. albicans* ACT1-GFP within the sample.

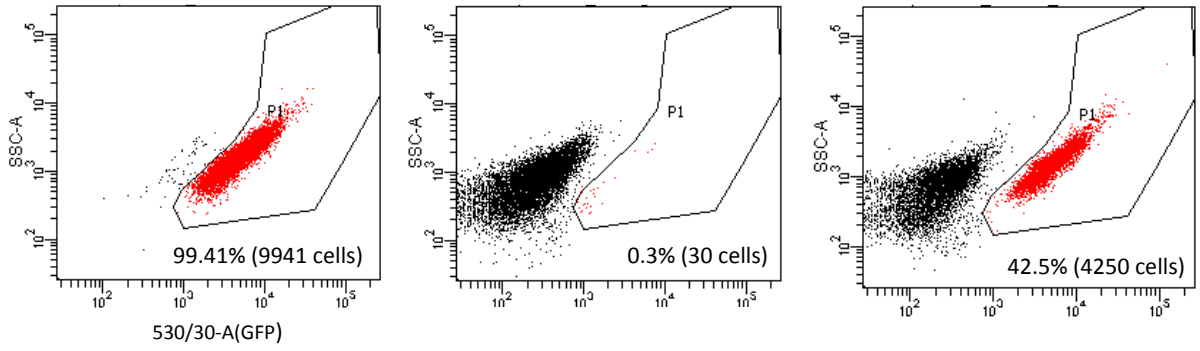

Supporting Fig. S1: Cells were analysed for green fluorescent protein (GFP) on a $530/30$ filter and side scatter by area. All plots show data for 10,000 detection events with the x-axis showing green fluorescent (GFP) intensity. From left to right we see the cytogram displaying *C. albicans* only, a GFP positive control; *C. glabrata* only, a non-fluorescent negative control, and a mixed culture of two species illustrating the clustering of two populations in mixtures. Populations were gated (P1) based on analysis of axenic cultures of C. albicans and C. glabrata so that the gated region successfully discriminated *C. albicans* from *C. glabrata* with a false positive detection rate within the gated region of $< 1\%$, as shown in each figure.

1.5 Long-term competition of *C. albicans* and *C. glabrata* for different drug regimes

Overnight cultures in YPD of *C. albicans* and *C. glabrata* were diluted, counted on hemocytometer, and adjusted a 1:1 ratio of each species, at a final concentrations of 2×10^7 cells/mL in SC medium containing either 0.1, or 4% (weight/volume) glucose. The cell suspension was then diluted 1:1 in SC media containing two times desired fluconazole concentration ($3\,\mu g/mL$) and the matching glucose concentration, to a final volume of $150\,\mu L$ in a 96 well flat bottom microtiter plate. Plates were sealed using sterile adhesive films, two holes were punched in seal above each well using a sterile

needle, and incubated overnight in orbital shaker set at 30^oC, 180 rpm. Each treatment was repeated in triplicate. After 24 hour incubation period (one season) plates were opened, the contents of the well were vigorously pipetted to achieve a homogenous cell suspension, and five microliters of cell suspension was added to a new well containing $145\,\mu$L of SC media which contained either the same, or a reduced concentration of glucose and fluconazole. Specifically, for treatment α the cultures were maintained in 0.1% glucose throughout, while the fluconazole concentration was adjusted each season ($3, 2, 1, 0.5, 0\,\mu$g/mL). For treatment β the glucose concentration remained at 0.1% and fluconazole concentration at $0.5\,\mu$g/mL throughout the duration of the experiment. Lastly, for treatment γ both glucose and fluconazole concentrations were reduced each season, glucose decreasing from 4 to 0.1% ($4, 2, 1, 0.5, 0.1$) and fluconazole decreasing from 3 to $0\,\mu$g/mL ($3, 2, 1, 0.5, 0$). Note that 5μL represents the smallest volume transfer that ensures the accuracy of pipetting is maintained. The relative frequency of *C. albicans* was monitored either by flow cytometry or CFUs, as described above. For daily monitoring $9-12$ replicate biological samples were measured, while at the endpoint all replicates were analysed (48 replicates for treatment α, 96 replicates for treatment β and 55 replicates for treatment γ).

1.5.1 Oscillatory (a repeated on-off) drug treatment

Overnight cultures in YPD of *C. albicans* and *C. glabrata* were diluted, counted on hemocytometer, and adjusted a 1:1 ratio of each species, at a final concentrations of 2×10^7 cells/mL in SC medium containing 0.1% (weight/volume) glucose. The cell suspension was then diluted 1:1 in SC media containing two times desired fluconazole concentration (0, 2, or $4\,\mu$g/mL) to a final volume of $150\,\mu$L in a 96 well flat bottom microtiter plate. Plates were sealed using sterile adhesive films, two holes were punched in seal above each well using a sterile needle, and incubated overnight in orbital shaker set at 30^oC, 180 rpm. Each condition was repeated in triplicate. After 24 hour incubation period (one season) plates were opened, the contents of the well were vigorously pipetted to achieve a homogenous cell suspension, and five microliters of cell suspension was added to a new well containing $145\,\mu$L of SC media which contained the same drug concentration as the day prior, for three days. At day three through day 14, cells were cultured without drug. On day 14 all conditions were treated with $2\,\mu$g/mL fluconazole for an additional three day (through day 17) at which point drug was again omitted from culturing through end of experiment. All wells were passaged daily, on days with data points shown in Figure 1a a volume of suspension was removed for sampling. To monitor relative frequency of each *Candida* species, colony forming units (CFU) were enumerated by plating on YPD agar either with or without the *C. albicans* strain selection nourseothricin (NAT) at $200\,\mu$g/mL. Briefly, cell suspension from overnight culture was diluted to roughly 200 CFU/ $100\,\mu$L and plated on both YPD and YPD+NAT plates, each well was plated in duplicate. Plates were incubated at 30^oC for 48 hours and colonies counted, with the percent *C. albicans* being determined by the ratio of NAT resistant cells to total cells on untreated YPD plates.

1.6 Intracellular fluconazole accumulation

The accumulation of fluconazole for both *C. albicans* and *C. glabrata* was analyzed in energized cells in the presence of glucose using the protocol described in (*65*). Cells were incubated with [^{3}H]-FLC (specific activity 740 GBa/mmol, 20 Ci/mmol, 2×10^4 CPM/pmol, $1\,\mu$Ci/ μL; $50\,\mu$M FLC; custom synthesis by Amersham Biosciences, UK). Cells were grown overnight in CSM complete medium at 30°C to a density typically between OD_{600} 6.0 to 8.0, unless otherwise noted. Cells were subsequently

harvested by centrifugation ($3000\times$ g, 5 m) and washed three times with YNB complete (1.7 g yeast nitrogen base without amino acids or ammonium sulfate, 5 g ammonium sulfate per liter, pH 5.0) without glucose (for starvation) and without supplementation, unless otherwise noted. Cells were resuspended at an OD_{600} of 75 in YNB for $2-3$h for glucose starvation. Reaction mixes consisted of $250\,\mu$L of YNB, $200\,\mu$L of cells (75 OD) and $50\,\mu$L of [^{3}H]-FLC ($1/100$ dilution of stock). The resulting [^{3}H]-FLC concentration is 50 nM ($0.015\,\mu$g/mL), which is significantly below the MIC for all strains. Samples ($100\,\mu$L) were removed at various time points and placed into 5 ml stop solution (YNB $+20$ mM [$6\,\mu$g/mL] FLC), filtered on glass fibre filters (24 mm GF/C; Whatman; Kent, UK) pre-wetted with stop solution and washed with 5 ml of stop solution. Filters were transferred to 20 ml scintillation vials. Scintillation cocktail (Ecoscint XR, National Diagnostics, Atlanta GA) was added (15 ml) and the radioactivity associated with the filter was measured with a liquid scintillation analyzer (Tri-Carb 2800 TR; Perkin Elmer; Waltham, MA) and normalized to CPM$/1\times10^8$ cells. Rate of [^{3}H]-FLC uptake was determined by incubating samples in the presence of increasing concentrations of unlabeled FLC (unless otherwise noted) and samples were analyzed for [^{3}H]-FLC accumulation at designated time points.

1.7 Dose-responses of *C. albicans* and *C. glabrata* to fluconazole

C. albicans is always substantially more responsive to drugs that *C. glabrata* irrespective of the glucose availability in the extracellular environment. This can be seen in Supporting Fig. S2 where using SC medium suplemented with either 1% or 4% glucose does not alter the relative ordering of the two species.

2 Dynamical systems theory: species coexistence

In dynamical systems theory, season number is a subscript n, so $f_{n+1}=\Phi(f_n)$ where $f_0=f$ is the *C. albicans* inoculum frequency. It follows by definition that $\Phi(0)=0$ because with no *C. albicans* in the inoculum, it can never appear. Similarly, $\Phi(1)=1$ must hold as a closed community containing only *C. glabrata* initially must always do so. For completeness, $G_{n+1}=1-\Phi(1-G_n)$ is the dynamical system describing the dynamics of *C. glabrata* frequencies ($G_n=1-f_n$).

Standard theory states that stable species coexistence occurs when Φ has a stable fixed point f_c, meaning $\Phi(f_c)=f_c$ and $-1<\frac{d\Phi}{df}(f_c)<1$. Here there is a value, $f_c\neq0$ or 1, of frequencies that remains unchanged after any number of seasons (Figure 2(c)). System bistability (whereby two long-term equilibrium outcomes are possible, depending on inoculum frequencies) at frequencies f_1 and f_2 occurs when $\Phi(f_1)=f_1,\Phi(f_2)=f_2,-1<\frac{d\Phi}{df}(f_1)<1$ and $-1<\frac{d\Phi}{df}(f_2)<1$ but $f_1\neq f_2$. 'Bistable exclusion' (either species can go extinct, depending on inoculum frequencies) arises when $f_1=0$ and $f_2=1$ in the definition of bistability and, when this occurs, theory tells us there is an *unstable* coexistence point f_u between 0 and 1 that satisfies $\left|\frac{d\Phi}{df}(f_u)\right|>1$ (Figure 2(d)). Time-dependent features of the community, even chaotic dynamics, can be deduced from the geometry of Φ. However, this geometry depends critically on the fluconazole (a) and glucose (g) supplied and we write $f_{n+1}=\Phi(f_n,a,g)$ to emphasise this, or $f_{n+1}=\Phi(f_n,a_n,g_n)$ when the fluconazole or glucose supplied changes each season.

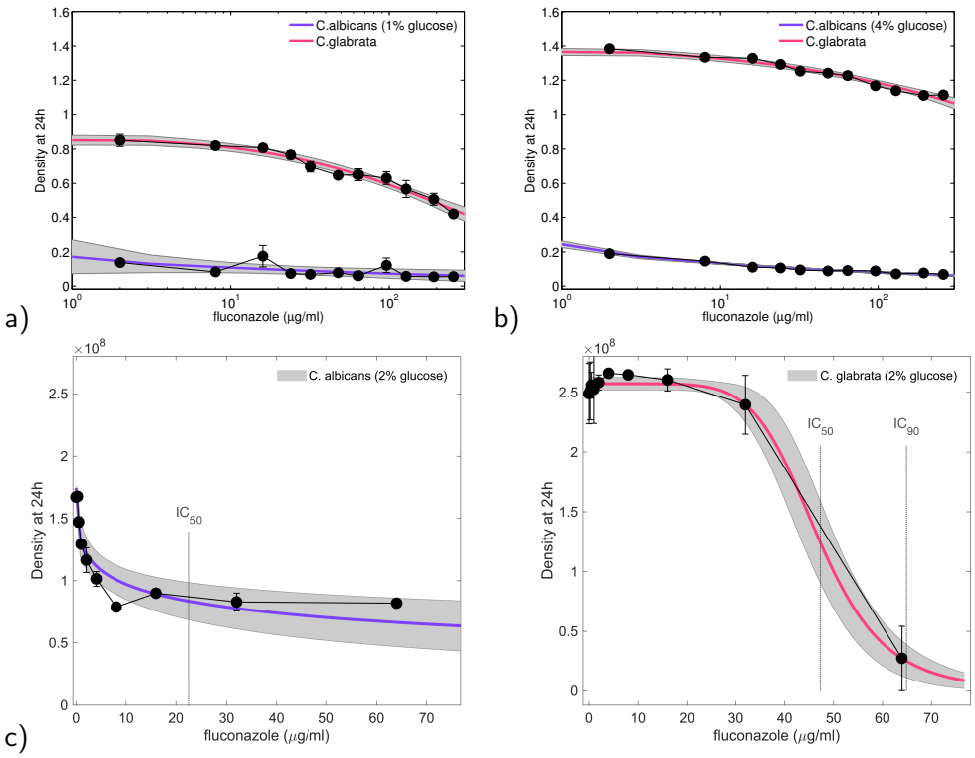

Supporting Fig. S2: Dose-response data at 24 hours for *C. albicans* and *C. glabrata* as monocultures in SC media supplemented with (a) 1% and (b) 4% glucose, for increasing fluconazole concentrations: dots are experimental data, best-fit Hill curves to data are black lines (grey lines: 95% confidence intervals) and density is stated in terms of 600nm optical density (turbidity). (c) Analogous data to (a) and (b), but at 2% glucose and density is determined by counting colonies. Note: (a) and (b) use a logarithmic x-axis with density measured as OD, (c) uses a standard x-axis with density measured as cells/ml. Data error bars are 95% CI of the mean, $n = 3$.

3 Bottom-up model development

To explore two species *C. albicans* and *C. glabrata* competition in an environment depending explicitly upon the extracellular concentration of an extracellular nutrient (glucose) and the concentration of fluconazole, we develop a simple metabolic model based on (*53*), and do not consider detailed metabolic properties of each species (*67*). In particular, the catabolism of this sugar and its intermediates is modelled as in (*53*), with a two-reaction process corresponding to glycolysis and the tricarboxylic acid (TCA) cycle. In the first reaction, sugar is taken from the environment and partially oxidized to form an intracellular metabolic intermediate, X_{in}, and n_1 molecules of ATP. In the second reaction, the intracellular intermediate is either completely oxidized to form CO_2 and n_2 molecules of ATP, or it passively diffuses out of the cell as an extracellular intermediate, X_{ex} with D representing a transport constant (*53*).

Since $n_1 < n_2$ this representation of sugar catabolism implicitly includes the rate-efficiency trade-off, known to play a crucial role in the outcome of resource competition amongst microorganisms (*53,63*). In our model the strength of the rate-efficiency trade-off constraining growth of one species depends on the presence of the competing species in the environment. For example, a Crabtree-positive *C.glabrata* (*66*) ferments most of the glucose to generate ethanol as bi-product (*67*). In the absence of competition from *C. albicans*, *C. glabrata* will eventually utilise ethanol as an additional energy

source once the glucose has been depleted. However, *C.albicans* is a Crabtree-negative species (*66*) that utilises most of its glucose through the TCA cycle to generate biomass and CO_2 (*67*). Therefore if present in the environment alongside *C.glabrata*, *C.albicans* competes for both glucose and ethanol, thus affecting *C.glabrata* growth rate and efficiency. These interactions are key to determining the two-species competition outcome, but are not captured by simpler models where the rate-efficiency trade-off is explicitly incorporated into the model (*63*).

We further assume that both catabolic reactions exhibit saturating enzyme kinetics so that the rates of ATP production during glycolysis, v_1, and the TCA cycle, v_2, are given by

$$v_1(S) = \frac{V_1 S}{K_1 + S}, \tag{1}$$

$$v_2(X_{in}) = \frac{V_2 X_{in}}{K_2 + X_{in}}, \tag{2}$$

where V_1 is the maximal uptake rate of resources in the glycolysis pathway and K_1 is the Michaelis-Menten constant. Similarly, V_2 denoted the maximal rate of CO_2 production in the TCA cycle pathway and K_2 its half-saturation constant. In addition we assume that the rate of cell growth is proportional to the rate of ATP production (*68*) according to a proportionality constant, G.

Despite the use of fluconazole in the clinic for decades, the basis of its antifungal mechanism is poorly understood (*69*). We assume that fluconazole growth suppression is the accumulation of processes that decrease per capita growth rate in a nonlinear and concentration-dependent manner, with greater inhibition at higher drug concentrations. We also assume that the inhibitory effect of fluconazole on growth depends only on the intracellular accumulation of the drug (*70*), not on the extracellular concentration. Therefore we represent reduction in growth rate by a function $0 \leq i(F_{in}) \leq 1$ which takes the form

$$i(F_{in}) = 1 - \frac{a(F_{in})^N}{b^N + (F_{in})^N} \tag{3}$$

where F_{in} and F_{ex} are the concentrations of intracellular and extracellular fluconazole respectively while a, b and N relate to the fluconazole resistance properties of the cell. Furthermore, we assume that fluconazole import into the cell is a saturating function of the extracellular fluconazole concentration of the form

$$I(F_{ex}) = \frac{V_i F_{ex}}{K_i + F_{ex}}, \tag{4}$$

where V_i is the maximal uptake rate of extracellular fluconazole in the fluconazole transporter pathway and K_i its half-saturation constant. In *C. albicans*, intracellular fluconazole concentration is known to saturate over 24 hours (*65*) and here we confirm the same finding for *C. glabrata* (Supporting Fig. S5). This suggests that the saturating import function is balanced by a saturating export function. Assuming that the rate of export is dependent on the intracellular accumulation of fluconazole (*71*), the export function takes the following form

$$E(F_{in}) = \frac{V_e F_{in}}{K_e + F_{in}}, \tag{5}$$

where V_e is the maximal rate of efflux in the efflux pathway and K_e its the half-saturation constant.

The dynamics of between-species competition for a fixed time period each season begins with the introduction of fluconazole (F_{ex}), glucose (S) and both species (C_a and C_g) into the environment and ends with the sugars exhausted, consumed during cell growth. The subscripts a and g throughout denote *C. albicans* and *C. glabrata*, respectively. One season of competition and pharmacodynamics is described by the differential equation (6). To mimic the dynamics of the laboratory microcosm in

the model, at the end of each season a fixed number of cells is transferred to a new environment that contains replenished growth medium, with glucose and fluconazole kept at the same concentration at the start of each season.

3.1 Model parameterisation

The following parameter values were taken from the literature: set $n_1 = 2$ pmol ATP/pmol glucose and $n_2 = 30$ pmol ATP/pmol X_{int} (*72*) while $D = 10^{-12}$ as in (*53*). The remainder were estimated below and are reported in Supporting Table S1.

3.1.1 Growth parameters

The growth kinetics parameters associated with *C. albicans* (*C. glabrata*), namely G_a, $V_{1,a}$, $K_{1,a}$, $V_{2,a}$ and $K_{2,a}$ (G_g, $V_{1,g}$, $K_{1,g}$, $V_{2,g}$ and $K_{2,g}$) were estimated by fitting numerical solutions of microbial population growth over time, determined using (6) with $C_g = F_{in} = F_{ex} = 0$ ($C_a = F_{in} = F_{ex} = 0$), to empirically obtained *C. albicans* (*C. glabrata*) growth data. The optimal parameter set was determined using two different methods: first, by optimising a root mean square (RMS) metric we obtain an initial guess that is then used as an input to the Markov Chain Monte Carlo (MCMC) Matlab Toolbox from where a maximum likelihood estimate (MLE), given the data and using uninformative priors, can be determined. Supporting Fig. S3 (a) shows the experimentally obtained growth curve for *C. albicans* over 24hours (black line) and the model fit using the optimised RMS values (blue line) and the MCMC MLE (red line). Both methods identify the same optimal parameter values and Supporting Fig. S3 (b) illustrates the estimated posterior marginal distributions determined using the MCMC toolbox. The fitted growth parameter values for *C. albicans* are listed in Supporting Table S1.

Supporting Fig. S4(a) shows an experimental growth curve dataset for *C. albicans* over 24 hours (black line) superimposed on top of which is the model fit determined using RMS optimisation (blue line) and the MCMC MLE (red line), posterior marginals of the MCMC chains are shown in Supporting Fig. S4 (b). In this case the RMS optimum differs significantly from the MLE estimate, with the RMS optimal parameter values corresponding to published values for *C. glabrata* (*66*) while the MLE optimal values corresponding to published values for the closely related species, *S. cerevisiae* (*66*), as illustrated in Supporting Fig. S4(c). This, to be consistent with known estimates for the species we are using, we chose to proceed with the RMS-determined parameter estimates for *C. glabrata* growth, these are listed in Supporting Table S1.

3.1.2 Drug transport and inhibition

The drug import/export parameters associated with *C. albicans* (*C. glabrata*), namely $V_{i,a}$, $K_{i,a}$, $V_{e,a}$ and $K_{e,a}$ ($V_{i,g}$, $K_{i,g}$, $V_{e,g}$ and $K_{e,g}$) were estimated by fitting the numerical solution of intracellular fluconazole accumulation, F_{in} described by the system (6) with $C_g = 0$ ($C_a = 0$), to the experimental data on *C. albicans* (*C.glabrata*) intracellular fluconazole accumulation. The optimal parameter set was determined using two different methods: first, by optimising a root mean square (RMS) metric we obtain an initial guess that is then used as an input to the Markov Chain Monte Carlo (MCMC) Matlab Toolbox from where a maximum likelihood estimate (MLE) was obtained. Given this modelling construct, the MLE fit converged to a parameters set with non-physical characteristics and therefore we chose to proceed with the RMS-determined parameter estimates with the experimental data and

the model fit shown in Supporting Fig. S5 and the optimal parameter values presented in Supporting Table S1.

The drug inhibition parameters associated with *C. albicans*, namely a, b and n (see equation (3)) were estimated in the following way. The dose-response curve showing the final population density at 24 hours generated by (6) with $C_g = 0$ for different initial drug concentrations ($0 - 64\mu$g/ml) was fitted to the experimentally obtained *C. albicans* dose-response data. The optimal parameter set was determined as a MCMC MLE estimate using the MATLAB MCMC Toolbox with the results illustrated in Supporting Fig. S6(a) and the best fit parameter values given in Supporting Table S1. For *C. galbrata* no inhibition of the growth was detected for a range of drug concentrations ($0 - 32\mu$g/ml) with inhibition observed only at the final concentration of 64μg/ml (Supporting Fig. S6). Therefore for *C. glabrata* we set $i(F_{in}) = 1$ and note that prediction of the competition outcomes and the subsequent experimental tests were conducted at fluconazole concentrations well below 64μg/ml. Note that while fluconazole concentrations in the model simulations are represented in [pmol/ml] they are reported in [μg/ml] after conversion.

Supporting Table S1: Maximum likelihood model parameter values.

Parameters	*C. albicans*	*C. glabrata*
V_1 [pmol/cell/min]	0.017999	0.1
K_1 [pmol/ml]	4.1652×10^6	22×10^7
V_2 [pmol/cell/min]	0.29767	0.1
K_2 [pmol/ml]	5.4323×10^9	4×10^9
G [cell/pmol ATP]	0.042412	0.066
V_i [pmol/cell/min]	655×10^{-11}	9.8×10^{-9}
K_i [pmol/ml]	6×10^4	1.6×10^4
V_e [pmol/cell/min]	2×10^{-11}	3.9×10^{-11}
K_e [pmol/cell/min]	5.8	0.7
a	0.52059	n/a
b [pmol/ml]	12.001	n/a
n	5.2347	n/a

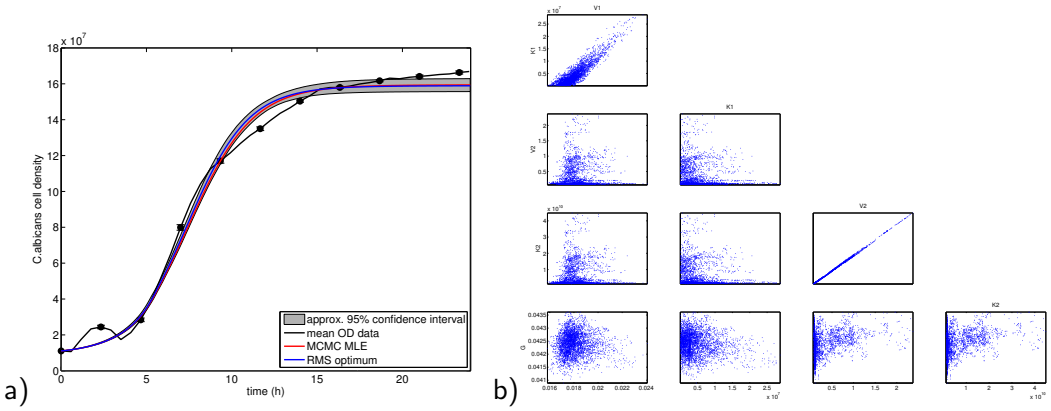

Supporting Fig. S3: (a) Growth of *C. albicans* (cells/ml) over a single season (24 h) in SC medium containing 2% glucose and in the absence of drugs (error bars are mean $\pm$ standard error, $n = 6$). The black line represents experimental data, while the best fits for the model (6) with $C_g = F_{in} = F_{ex} = 0$, are shown in red (a MCMC MLE) and blue (a RMS local optimum). The grey areas in the plot correspond to 95% confidence interval for the MCMC MLE; (b) Posterior marginal distributions determined using the Matlab MCMC toolbox for the five fitting parameters plotted in a pairwise fashion

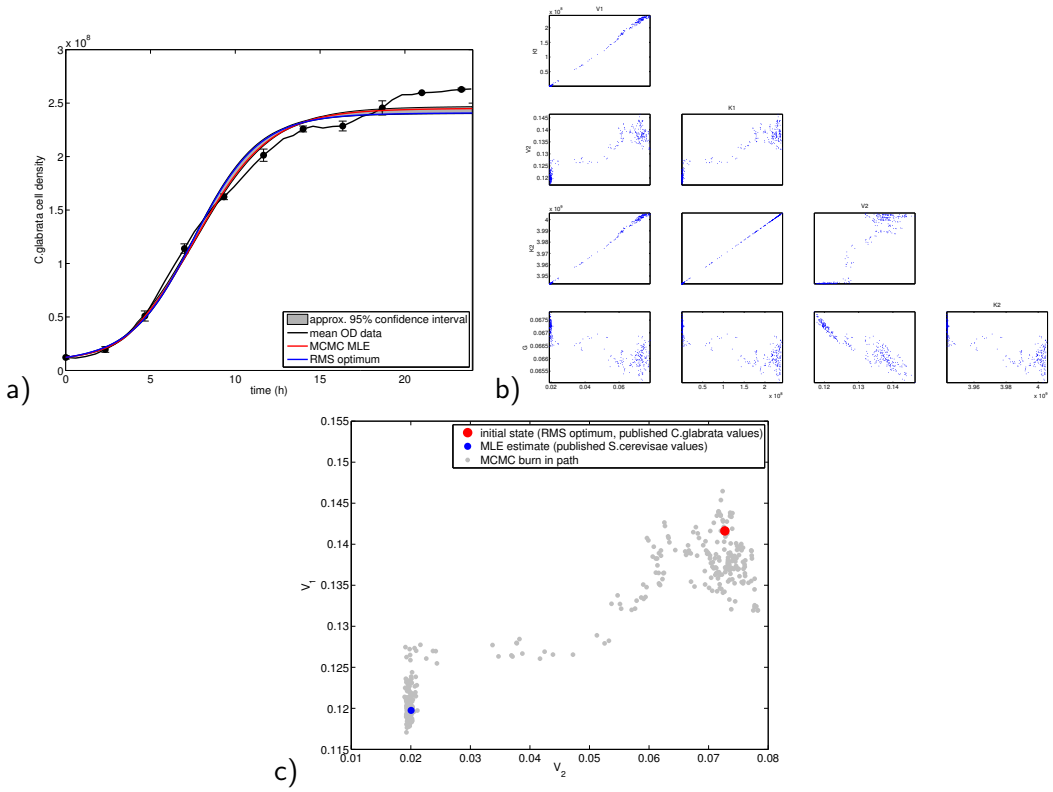

Supporting Fig. S4: (a) Growth of *C. glabrata* (cells/ml) over a single season (24 h) in SC medium containing 2% glucose and in the absence of drugs (error bars are mean $\pm$ standard error, $n = 6$). The black line represents experimental data, while the best fits for the model (6) with $C_a = F_{in} = F_{ex} = 0$, are shown in red (a MCMC MLE) and blue (a local RMS optimum). The grey areas in the plot correspond to 95% confidence interval for the MCMC MLE; (b) estimated posterior marginal distributions from the computed MCMC chains for the five fitting parameters, plotted in a pairwise fashion; (c) a typical burn-in trajectory of the MCMC Metropolis-Hastings algorithm plotted in (V_1, V_2)-space, showing the initial state (a local RMS optimum, red dot) corresponding to published values for *C. glabrata* and the MLE estimate corresponding to published values for *Saccharomyces cerevisiae* (blue dot).

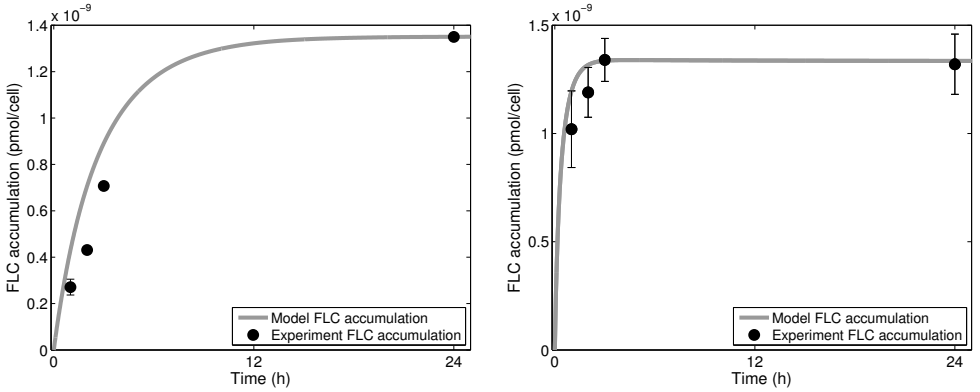

a) *C. albicans* b) *C. glabrata*

Supporting Fig. S5: Intracellular fluconazole accumulation for (a) *C. albicans* and (b) *C. glabrata*. The black dots represent experimental data (error bars are mean $\pm$ standard error, $n = 3$), while the grey line represents a locally optimal RMS fit of the model (6) with $C_g = 0$ ($C_a = 0$) to *C. albicans* (*C.glabrata*) data. To reflect the experimental environment our initial environment contains 2% w/v glucose and a low concentration of fluconazole, namely 0.015μg/ml that does not have a significant inhibitory effect on the microbial population . The initial cell density for *C. albicans* species is set to $C_a(0) = 12.8 \times 10^8$ (cells/ml), while the initial cell density for *C.glabrata* species is set to $C_g(0) = 13.6 \times 10^8$ (cells/ml).

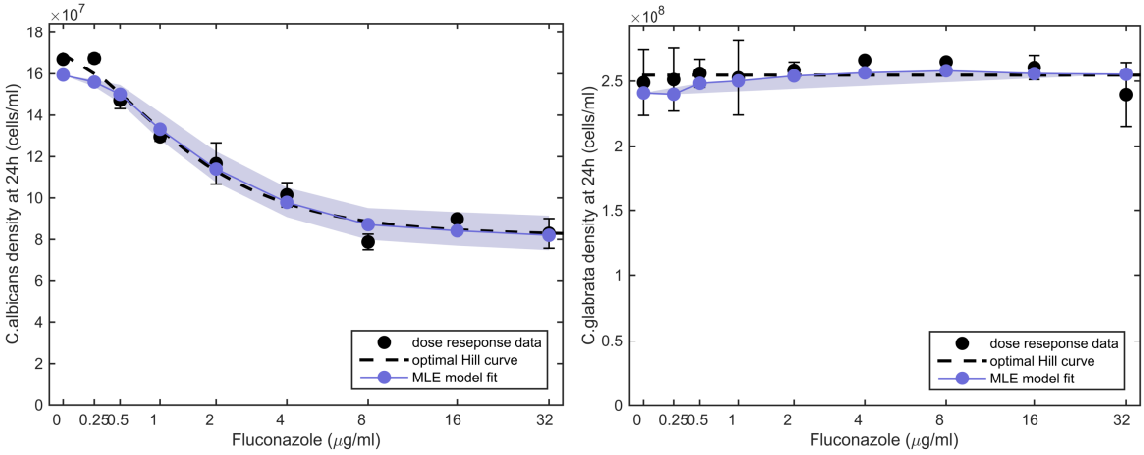

a) *C. albicans* b) *C. glabrata*

Supporting Fig. S6: Dose response curve at 24 hours for (a) *C. albicans* and (b) *C. glabrata* in response to increasing fluconazole. Black dots represent experimental data. The MLE model fit is plotted in blue while the optimal Hill curve for the *C. albicans* dose-response is shown as a black dashed line. Error bars are estimated for model fits and show mean standard error, $n = 3$ for data.

3.2 The theoretical model statement: $\Phi(f, a, g)$ in detail

To explore the dependence of a theoretical community of two Candida species on antibiotic and extracellular nutrients, we studied a mathematical model of Φ and its dynamics. *C. albicans* and *C. glabrata* respond differently to both fluconazole (Supporting Fig. S2) and glucose (Supporting Fig. S3(a), Supporting Fig. S4(a)) so the model describes two-species frequency- and density-dependent competition in environments that explicitly depend upon extracellular glucose and fluconazole. Accordingly, sugar catabolism is modelled (as elsewhere (*53*)) using a coarse-grained, two-reaction representation of glycolysis and the TCA cycle. The first reaction occurs at rate v_1 where glucose is imported and partially oxidized to form an intracellular metabolic intermediate, X_{in}, and n_1 molecules of ATP. The second reaction occurs at rate v_2 with the intracellular intermediate either completely oxidized to form CO_2 and n_2 molecules of ATP, or it passively diffuses out of the cell as an extracellular intermediate, X_{ex} with D representing a diffusion constant (*53*).

The dynamics of between-species competition in each season begins with the introduction of fluconazole (F_{ex}) and glucose (S) while observing the densities of both species (C_a and C_g) in the environment; subscripts a and g denote *C. albicans* and *C. glabrata*, respectively. Extracellular fluconazole (F_{ex}) is imported into the cell at a rate I, while intracellular fluconzole F_{in} is exported out of the cell and into the environment at a rate E, with i denoting a drug inhibition function which depends on F_{in}.

Subsequently, one season of competition is described by the following differential equation (see Supporting Information 3 for parameterisation):

$$\frac{dS}{dt} = -v_{1,a}(S)C_a - v_{1,g}(S)C_g, \tag{6a}$$

$$\frac{dX_{ex}}{dt} = D(X_{in,a} - X_{ex})C_a + D(X_{in,g} - X_{ex})C_g, \tag{6b}$$

$$\frac{dC_a}{dt} = G_a \cdot i(F_{in,a}) \left[v_{1,a}(S)n_1 + v_{2,a}(X_{in,a})n_2)\right] C_a, \tag{6c}$$

$$\frac{dC_g}{dt} = G_g \cdot i(F_{in,g}) \left[v_{1,g}(S)n_1 + v_{2,g}(X_{in,g})n_2)\right] C_g, \tag{6d}$$

$$\frac{dX_{in,a}}{dt} = \left[-D(X_{in,a} - X_{ex}) + v_{1,a}(S) - v_{2,a}(X_{in,a})\right] C_a, \tag{6e}$$

$$\frac{dX_{in,g}}{dt} = \left[-D(X_{in,g} - X_{ex}) + v_{1,g}(S) - v_{2,g}(X_{in,g})\right] C_g, \tag{6f}$$

$$\frac{dF_{in,a}}{dt} = (I(F_{ex}) - E(F_{in,a}))C_a, \tag{6g}$$

$$\frac{dF_{in,g}}{dt} = (I(F_{ex}) - E(F_{in,g}))C_g, \tag{6h}$$

$$\frac{dF_{ex}}{dt} = (E(F_{in,a}) - I(F_{ex}))C_a + (E(F_{in,g}) - I(F_{ex}))C_g. \tag{6i}$$

To mimic the laboratory microcosm at the end of each season a fixed number of cells is transferred to a new environment containing replenished growth medium with glucose and fluconazole at the same concentration at the start of each season. To form the map $\Phi(f, a, g)$, we set $f = C_a(0)/(C_a(0) + C_g(0))$ and solve the differential equation (6a-i) setting $F_{ex}(0) = a, X_{ex}(0) = g$ for $T = 24h$ units of time, then $F = C_a(T)/(C_a(T) + C_g(T))$ *is* the value of $\Phi(f, a, g)$.

4 Irreversible community dynamics

We can now present a technical mechanism supporting irreversible community dynamics following drug withdrawal. Suppose that a model system, $\Phi(f, a, g)$, satisfies the following axioms: (1) it possesses bistable exclusion for all $a \geq 0$ and $g > 0$; (2) $f = 0, f = f_u$ and $f = 1$ are the only solutions (fixed points) of

$$f = \Phi(f, 0, g), \tag{7}$$

with unknown f, for any $g \geq 0$. (3) f_u (whose value depends on g) is an unstable coexistence point when $a = 0$ and (4) $a_1 > 0, ..., a_N > 0$ are drug dosages for a treatment that eventually stops, so $0 = a_{N+1} = a_{N+2} = a_{N+3} = ...$; thus our model is a discrete map that is eventually autonomous.

Now suppose (g_n) is a sequence of glucose dosages and $f_0 > f_u(g_0)$ but $f_N < f_u(g_N)$, where f_N is the N-th element of the sequence $f_{n+1} = \Phi(f_n, a_n, g_n)$. Then, the two sequences

$$\overbrace{f_{n+1} = \Phi(f_n, 0, g_n)}^{\text{no drug ever given}} \qquad \text{and} \qquad \overbrace{f_{n+1} = \Phi(f_n, a_n, g_n)}^{\text{drug treatment eventually stops}}$$

will satisfy $f_n \to 1$ (*C. albicans* dominates) in the former but $f_n \to 0$ (*C. glabrata* dominates) in the latter, as $n \to \infty$. Mathematically, these conditions describe a treatment-induced tipping point determined by $f_u(g)$ (see §4.1 below) whereby the use of antibiotic, albeit only for N seasons, forces dynamics towards the 'separatrix' $f_u(g)$ and if this point is passed during treatment, or not, different species will dominate long-term.

4.1 Illustration of a tipping mechanism

To illustrate the existence of a treatment induced tipping point, suppose that the frequency dynamics of *C. albicans* are given by the dynamical system

$$f_{n+1} = \Phi(f_n, a, g)$$

where a is the fluconazole extracellular supply concentration and g is the glucose supply concentration. If we set the *C. glabrata* frequency to be $G_n = 1 - f_n$ then

$$G_{n+1} = 1 - \Phi(1 - G_n, a, g)$$

follows. Given a sequence of treatments, (a_n, g_n), then the non-autonomous system $f_{n+1} = \Phi(f_n, a_n, g_n)$ describes the system's dynamics.

Supporting Fig. S7 indicates what can happen when a_n alternates periodically between 'on' (meaning $a_n > 0$) and 'off' ($a_n = 0$) treatment states when *competitive exclusion* holds between the two organisms. In this case the repeated application and withdrawal of the drug leads to cyclical dynamics between the two pathogens, oscillating between the near-exclusion of either species through time.

However, now suppose that the system response to the drugs differently so that when $a = 0$ competitive exclusion still applies, but when $a > 0$ a 'bistable exclusion' condition applies. Supporting Fig. S8 gives the geometry of Φ in this case, written in terms of $1 - \Phi(1 - G, a, g)$ with G on the x-axis. It is now possible for tipping behaviour to occur because the drug-treated state has an unstable fixed point labelled f_u (and we also write $f_u = 1 - G_u$) in the main text. If it happens to be the case that the system is treated with drug for a while and during that treatment f_n (or G_n) moves from one side of the tipping point to the other, it is in this situation that irreversible dynamics will occur following drug withdrawal.

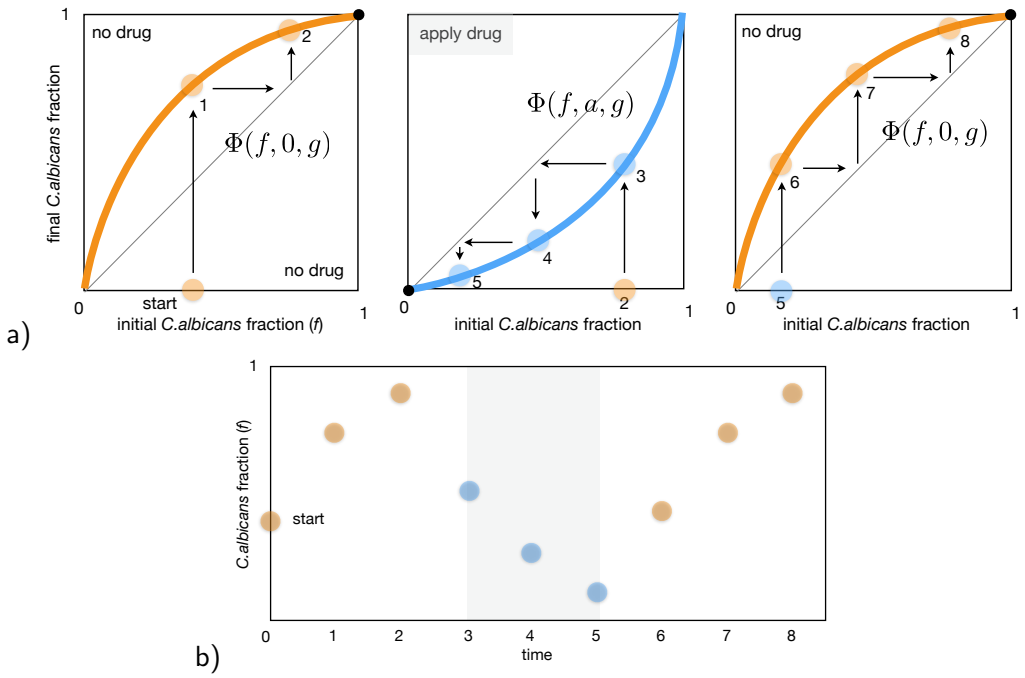

Supporting Fig. S7: This shows a typical reversible drug-treatment dynamic first with no drug given, then the application and, finally, the withdrawal of the drug. In a), the community is described by the map $f_{n+1} = \Phi(f_n, a, g)$ where a has been set to zero. In the middle such plot the dynamical system describing the community is $f_{n+1} = \Phi(f_n, a, g)$ where a is now positive, and the rightmost plot again has $f_{n+1} = \Phi(f_n, 0, g)$ as its dynamical model. When $a = 0$ the model selects for *C.albicans* whereas when $a > 0$ it selects for *C.glabrata* and the off-on-off sequence of the drug treatment sees the frequency of *C.albicans* oscillate in the community, as shown in b).

The conditions alluded to above merely give one possible set of sufficient conditions for tipping to occur, there are many other of analogous conditions describing situations whereby tipping behaviour will arise and some of these may lead to tipping more readily than the above conditions indicate. For example, if we are able to vary *both* a and g simultaneously then the two-parameter (i.e. codimension two) variation is able to encounter a tipping curve rather than a tipping point.

To formalise this a little, consider the non-autonomous system

$$f_{n+1} = \Phi(f_n, a_n, g_n)$$

and suppose the fixed-point equation $f = \Phi(f, a, g)$ has a nontrivial, unstable (i.e. $f \notin \{0, 1\}$) fixed point that depends *both* on a and g. Write the solution of this equation $f = f_u(a, g)$ and note, therefore, that $f_u(0, g)$ is a function of g alone that describes the variation of a tipping point with respect to change in glucose availability for the untreated dynamical system. Now, when the drug treatment is removed, meaning $a_n = 0$ for all $n \geq N$, for some N, if the sequence of states (f_n) manages to approach or else traverse the value $f_u(0, g_n)$ at some value of n, whether from above to below or vice versa, then tipping behaviour will become apparent. This additional parametric freedom makes tipping points potentially easier to locate from an empirical perspective because of the additional parametric freedom when compared with experimental systems that hold glucose, g, constant throughout. Moreover, as Figure 1 shows in the main text, we were not able to locate tipping behaviour unless we varied *both* a and g as part of the treatment protocol. This is not to say that tipping points do not exist in our laboratory community with respect to variation only in a,

but given the small number of parametric states that can be searched for tipping behaviour, we were only able to observe tipping when both a and g were varied together, as a was withdrawn.

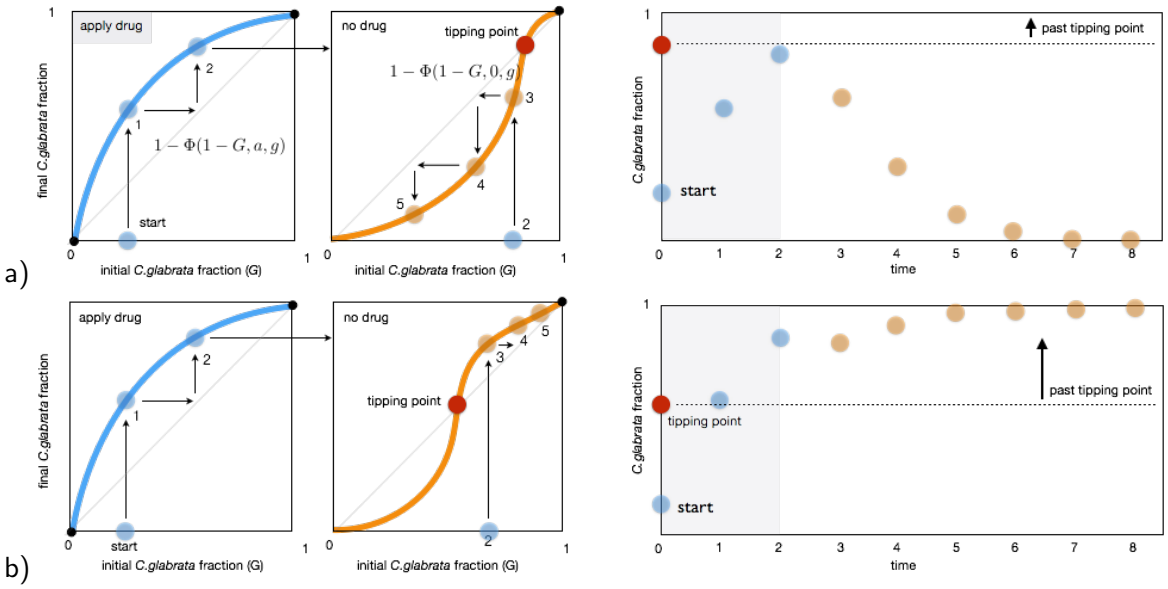

Supporting Fig. S8: We now write $G_n = 1 - f_n$, where G_n is the frequency of *C.glabrata* in the community, so $G_{n+1} = 1 - \Phi(1 - G_n, a, g)$ is the dynamical system that describes the community's dynamics from the perspective of *C. glabrata*. a) This shows a reversible on-off drug treatment dynamic whereby the initial application of the drug selects for *C.glabrata* but the sytem trajectory get very close to the unstable fixed point f_u without actually quite breaching it. As a result, when the drug is withdrawn, *C.glabrata* rescinds. However, b) shows a different set of dynamics for the same type of map Φ whereby, in this case, the drug dose $a > 0$ has the property that the tipping point (red dot) is breached after one or two drug treatments. As a result, when the drug is removed *C.glabrata* continues to dominate and, as a result, *C.albicans* may be eventually lost from the community.

Figure S9 below now illustrates how a tipping point arises in replicates of the community dynamics in the case, like treatment γ, whereby fluconazole and glucose concentrations are reduced.

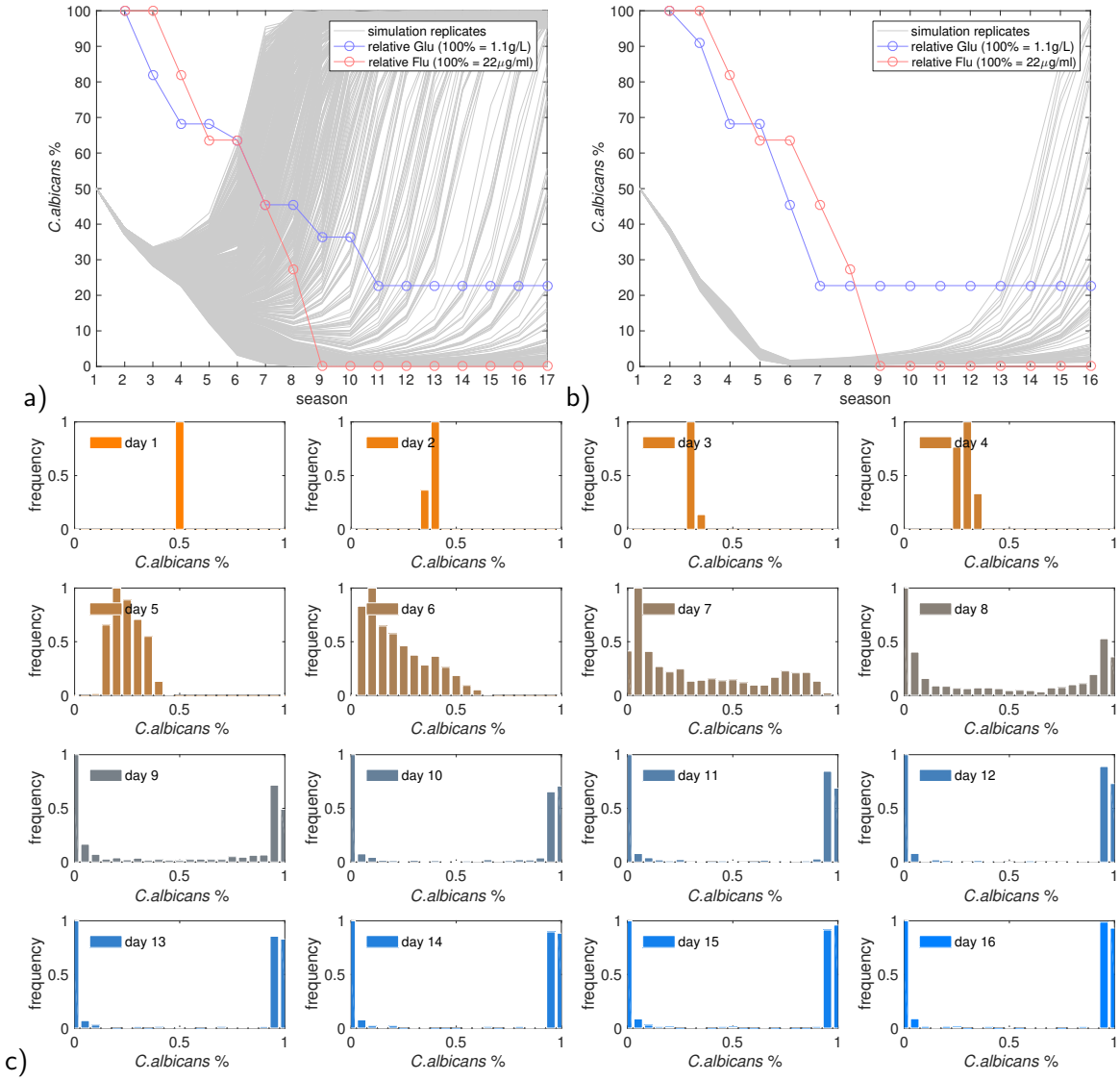

Supporting Fig. S9: a) Shown are 1000, 17-day replicate computer-simulated trajectories where the fluconazole and glucose changes are indicated by the legend: the replicates diverge markedly on days 5 and 6 before drug treatment ends. b) This is an analogous set of computational simulations to a) but where, with a subtly different change in environmental conditions, the tipping point only occurs after the drug treatment has ended. c) This shows histograms of community configurations for each day of the simulations taken from the data in a). This also shows how an initial community seeded with 50% of each of the two Candida species soon diverges into a set of communities with very different configurations, as reflected by the increase in variance and change in form of the histograms that reflects what is observed empirically in Figure 4(c). When we extend the simulations for sufficient time, here 16 days, we observe two distinct types of community come to dominate with very different species, and therefore, resistance profiles.

5 Appendix - Additional Figures

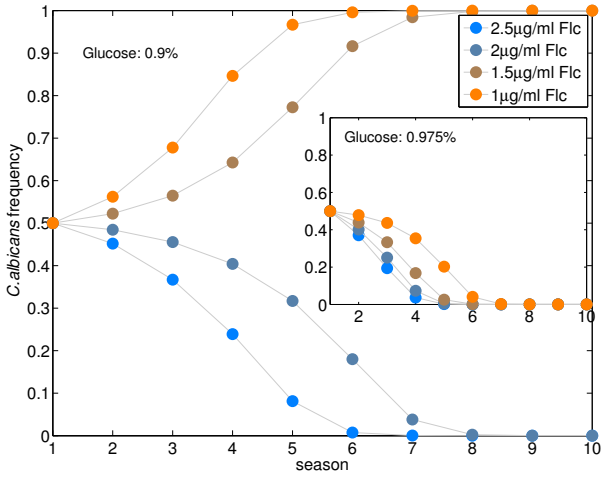

Supporting Fig. S10: Analogous to Figure 3(a) in the main text but here tipping points in system dynamics are observed with respect to small changes in glucose availability as can be seen by comparing dynamics in the main plot with those in the inset, noting the glucose supply percentage in each case.

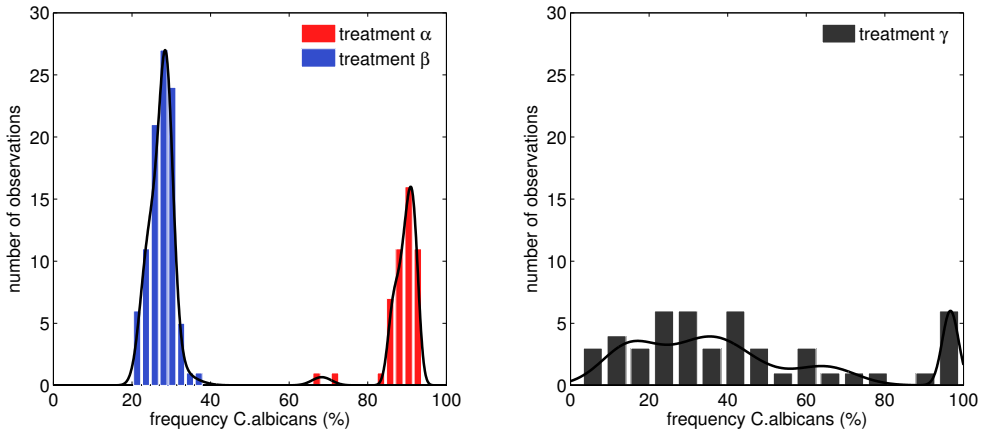

Supporting Fig. S11: Additional analysis for Figure 4: histograms of observed *C.albicans* frequencies in communities undergoing treatments α, β and γ (defined in the main text) on the last season of each treatment and AIC-optimal Gaussian mixture models are fitted to data. The three resulting plots (in red, blue and black) also show (as three black lines) a summation of two Gaussians are optimal for treatment β (one isn't sufficient because of skew), three are optimal for α because of the datapoints outside the main cluster, whereas five Gaussians are optimal for treatment γ because of a much wider support of the data. These data are taken from 48 replicates for treatment α, 96 for β and 55 for γ.

Figure S12 below refers to 'diffusion theory' associated with the data in Figure 4. By this we mean that if a collection of m replicate timeseries, $f_j(t)$, of *C.albicans* percentages in the community is known on days $t = 1, 2, ..., N$ (t denoting time), then define the mean percentage each day $\mu(t) = \sum_{j=1}^{m} f_j(t)/m$. If the *C.albicans* percentages are assumed to follow some, possibly deterministic

(e.g. defined by some underlying dynamical system), trajectory or signal, $s(t)$, subject to additive but zero-mean noise generated by a random walk, $\sigma(t)$, then $\mu(t) \approx s(t)$ (with better approximation for larger m as described by the central limit theorem) and the diffusion equation predicts the mean deviation of $\{f_j(t)\}$ from $s(t)$ would be approximated by $\sigma \cdot t^{1/2}$ for some noise constant, σ. As the triangle inequality states that between-replicate variation is less than $2\times$ standard deviation, we fitted BRV versus time data against power laws of the form $\sigma \cdot t^p$ where p and σ are unknown fitting parameters. We say that data is consistent with diffusion theory if the hypothesis that $p = 1/2$ cannot be rejected. If $p > 1/2$ according to this fit, we say that the data is super-diffusive. As Figure S12 explains, treatments α and β are consistent with diffusion theory (although a more likely model of the dynamics of the BRV data is available for α) whereas treatment γ (for which we claim tipping behaviour) is super-diffusive.

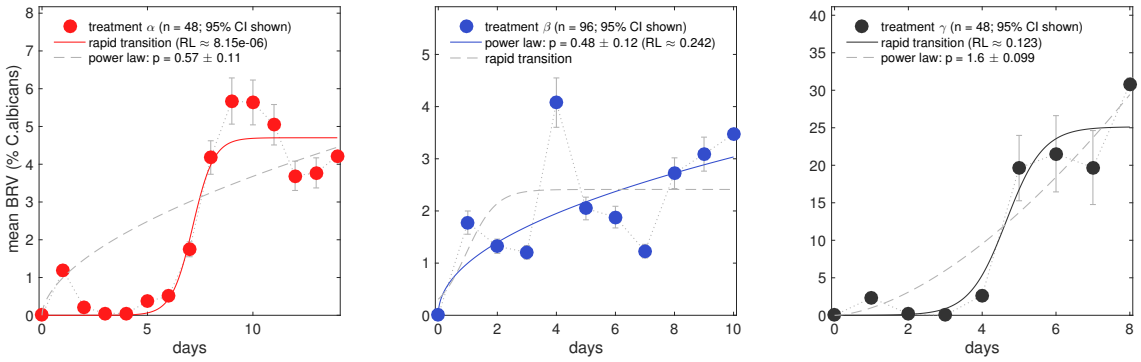

Supporting Fig. S12: Additional analysis for Figure 4. We asked whether the replicate trajectories of treatments α, β or γ diverged in manner consistent with the theory of diffusive random walks and continuous (but rapid) transitions. For this we fitted two mathematical models against between-replicate variation (BRV) data: a power law (where diffusion theory predicts the power, p, equals $1/2$) and a Hill-type function that can capture rapid, continuous transitions between states. The most likely of the fits (based on AIC relative likelihoods (stated as RL)) is shown for each treatment as a thick, coloured line whereas the least likely model is shown as a dashed line. The most likely model for treatment α in red is the rapid transition model which transitions on days 6,7 and 8, approximately by just 5 *C. albicans* % units and this data has a (less likely) power law fit where $p \approx 0.57 \pm 0.11$ (95% CIs). Thus, this data is consistent with diffusion theory although a change by 5% over a 3-day period is the more likely model. Treatment β in blue, on the other hand, is better described by diffusion theory where $p \approx 0.48 \pm 0.12$. Treatment γ for which we claim tipping is super-diffusive ($p \approx 1.6 \pm 0.1$) and the more likely model of BRV, namely the rapid transition datafit, increases by approximately 20% units from day 4 to 5.

Supplementary References

64. S. W. Milne, J. Cheetham, D. Lloyd, S. Aves, S. Bates, *Yeast* **3**, 833 (2011).

65. B. E. Mansfield, *et al.*, *PLoS Pathogens* **6**, 11 (2010).

66. H. van Urk, E. Postma, W. a. Scheffers, J. P. van Dijken, *Journal of general microbiology* **135**, 2399 (1989).

67. I. V. Ene, S. Brunke, A. J. P. Brown, B. Hube, *Cold Spring Harb Perspect Med* **4**, a019695 (2014).

68. T. Bauchop, S. R. Elsden, *Journal of General Microbiology* **23**, 457 (1960).

69. Y.-Q. Zhang, *et al.*, *PLoS pathogens* **6**, e1000939 (2010).

70. P. Marichal, J. Gorrens, M. C. Coene, L. Le Jeune, H. Vanden Bossche, *Mycoses* **38**, 111 (1995).

71. D. G. Thanassi, L. W. Cheng, H. Nikaido, *Journal of bacteriology* **179**, 2512 (1997).

72. S. Dagley, D. E. Nicholson, *An introduction to metabolic pathways*, Blackwell scientific publications (Blackwell Scientific Publications, 1970).